Impact of membrane lipid polyunsaturation on dopamine D2 receptor ligand binding and signalling

Marie-Lise Jobin[1]†, Véronique De Smedt-Peyrusse[1]†, Fabien Ducrocq[1], Rim Baccouch[2], Asma Oummadi[1], Maria Hauge Pedersen[3,4], Brian Medel-Lacruz[5], Maria-Florencia Angelo[1], Sandrine Villette[2], Pierre Van Delft[6], Laetitia Fouillen[6], Sébastien Mongrand[6], Jana Selent[5], Tarson Tolentino-Cortez[7], Gabriel Barreda-Gómez[7], Stéphane Grégoire[8], Elodie Masson[8], Thierry Durroux[9], Jonathan A. Javitch[3,4,10], Ramon Guixà-González[11]*, Isabel D. Alves[2]*, Pierre Trifilieff[1]*

[1] Université de Bordeaux, INRAE, Bordeaux INP, NutriNeuro, 33000, Bordeaux, France
[2] Institute of Chemistry & Biology of Membranes & Nanoobjects, CNRS UMR 5248, Université de Bordeaux, Bordeaux INP, 33600 Pessac, France
[3] Department of Psychiatry, Columbia University Vagelos College of Physicians and Surgeons, New York, NY 10032
[4] Division of Molecular Therapeutics, New York State Psychiatric Institute, New York, NY 10032
[5] Research Programme on Biomedical Informatics (GRIB), Hospital del Mar Medical Research Institute (IMIM)—Department of Experimental and Health Sciences, Pompeu Fabra University (UPF), 08003 Barcelona, Spain
[6] Laboratory of Membrane Biogenesis (LBM), Research Mix Unity (UMR) 5200, National Scientific Research Center (CNRS), University of Bordeaux, Bordeaux, France
[7] Research Department, IMG Pharma Biotech S.L., BIC Bizkaia (612), 48160 Derio, Spain
[8] Centre des Sciences du Goût et de l'Alimentation, AgroSup Dijon, CNRS, INRAE, Université Bourgogne Franche-Comté, 21000 Dijon, France
[9] Institut de Génomique Fonctionnelle, Université de Montpellier, CNRS, INSERM, Montpellier, France
[10] Department of Molecular Pharmacology and Therapeutics, Columbia University Vagelos College of Physicians and Surgeons, New York, NY 10032
[11] Condensed Matter Theory Group, Paul Scherrer Institute (PSI), 5232 Villigen PSI, Switzerland

† These authors contributed equally to this work
* Co-Senior authors
Corresponding authors: P. Trifilieff (pierre.trifilieff@inrae.fr) , I.D. Alves (i.alves@cbmn.u-bordeaux.fr), R. Guixà-González (ramon.guixa@psi.ch)

Abstract

Increasing evidence supports a relationship between lipid metabolism and mental health. In particular, the biostatus of polyunsaturated fatty acids (PUFAs) correlates with some symptoms of psychiatric disorders, as well as the efficacy of pharmacological treatments. Recent findings highlight a direct association between brain PUFA levels and dopamine transmission, a major neuromodulatory system implicated in the etiology of psychiatric symptoms. However, the mechanisms underlying this relationship are still unknown. Here we demonstrate that membrane enrichment in the n-3 PUFA docosahexaenoic acid (DHA), potentiates ligand binding to the dopamine D2 receptor (D2R), suggesting that DHA acts as an allosteric modulator of this receptor. Molecular dynamics simulations confirm that DHA has a high preference for interaction with the D2R and show that membrane unsaturation selectively enhances the conformational dynamics of the receptor around its second intracellular loop. We find that membrane unsaturation spares G protein activity but potentiates the recruitment of β-arrestin in cells. Furthermore, *in vivo* n-3 PUFA deficiency blunts the behavioral effects of two D2R ligands, quinpirole and aripiprazole. These results highlight the importance of membrane unsaturation for D2R activity and provide a putative mechanism for the ability of PUFAs to enhance antipsychotic efficacy.

Introduction

Biological membranes are not homogeneous bilayers but rather composed of different lipid species with various chemical and biophysical properties that actively modulate protein localization and function, signaling or vesicular trafficking [1]. However, several aspects of membrane complexity including the impact of lipid heterogeneity across tissues, cells, and subcellular compartments on cell signaling and physiology are only starting to emerge.

This is particularly true for neuronal function for which the impact of membrane lipid composition has been largely overlooked, despite the brain having the second highest lipid content after adipose tissue [2]. Yet, convergent findings support some links between lipid biostatus and mental health. For instance, a decrease in the levels of n-3 polyunsaturated fatty acids (PUFAs)-containing phospholipids has been consistently described in a subset of patients suffering from neurodevelopmental psychiatric diseases [3]. Likewise, various studies suggest alterations in common fatty acid metabolic pathways across several psychiatric disorders [4, 5]. Moreover, n-3 PUFA deficiency in rodent models has been associated with putative pathophysiological mechanisms involving alteration in neurogenesis, neuronal migration, neuromodulation, and neuroinflammatory processes in various brain regions [2, 6, 7]. These findings remain largely correlative and the precise mechanisms by which PUFA biostatus directly or indirectly accounts for changes in neuronal function remain largely unknown. Nevertheless, several studies have demonstrated that membrane lipids regulate the function of key transmembrane proteins [8] including ion channels and G protein-coupled receptors (GPCRs) [9, 10].

The activity of the dopamine D2 receptor (D2R) is particularly relevant in this context. Various psychiatric disorders, including those where levels of brain n-3 PUFAs are low, display altered patterns of D2R-dependent signaling [11], and this GPCR is, therefore, a key target in several pharmacological treatments. Similarly, different studies in rodent models show that n-3 PUFA deficiency affects dopamine transmission and related behaviors [12, 13]. In line with this evidence, we recently reported a unique vulnerability of D2R-expressing neurons to PUFA biostatus that directly accounts for the motivational deficits induced by n-3 PUFA deficiency [14]. Early experimental studies have reported that n-3 PUFAs, namely docosahexaenoic acid (DHA, 22:6), enhance the function of the prototypical class A GPCR rhodopsin [15–17]. Subsequent studies showed that DHA-containing phospholipids preferentially solvate rhodopsin [18, 19], which could impact receptor function. In addition, recent *in silico* studies [20, 21] demonstrate that the D2R also displays a preference for DHA interaction that could modulate receptor partitioning into specific membrane signaling platforms, as shown by early

97 experiments [22]. While these findings suggest that membrane PUFA composition could
98 influence the activity of the D2R, there is still no direct evidence for such an effect.
99

100 In this work, using both cell membrane extracts and model membranes, we found that DHA,
101 but not n-6 PUFA docosapentaenoic acid (DPA, 22:5), enhances D2R ligand binding affinity.
102 While DPA and DHA only differ in one double bond, molecular dynamics (MD) simulations
103 show that they have a strikingly different propensity for interacting with D2R. In addition, we
104 show that membrane unsaturation strongly influences conformational dynamics of the
105 receptor, notably of the second intracellular loop. Interestingly, membrane enrichment in either
106 DHA or DPA have no effect on agonist-induced, $G_{i/o}$ protein-dependent inhibition of cAMP
107 production. However, both DHA and DPA similarly enhance the maximal efficacy of the D2R
108 to recruit β-arrestin2 upon agonist stimulation. Finally, we provide *in vivo* evidence that
109 decreased membrane unsaturation with n-3 PUFA deficiency blunts the behavioral effects of
110 two D2R ligands, namely quinpirole and aripiprazole. Altogether, these data highlight the
111 impact of membrane PUFA composition on D2R activity and suggest that DHA acts as an
112 allosteric modulator of the receptor.

113

114 **Material and Methods**

115 **Chemicals**

116 Reagents, unless otherwise specified, were from Sigma-Aldrich (St. Louis, MO, USA) PUFAs
117 (Cis-4,7,10,13,16,19-DHA (DocosaHexaenoic Acid, ref D2534), DPA n-6 (DocosaPentaenoic
118 Acid, ref 18566) stock solutions (30 mM) were prepared in absolute ethanol under N2 [23]. For
119 anisotropy assays, LigandTag Lite D2 (L0002RED) receptor red antagonist was purchased
120 from Cisbio Bioassays. Quinpirole (ref 1061) and Forskolin (ref 1099) were from Tocris.

121

122 **Cell culture and treatment**

123 HEK 293 or CHO stably expressing the human D2R (Flp-in T-rex 293 SF-D2sWT/FRTTO 293)
124 were used. See supplementary information for details.

125 **Membrane preparation**

126 See supplementary information for the description of membrane preparation.

127

128 **Plasmon waveguide resonance (PWR)**

157   PWR experiments were performed with a homemade instrument equipped with a He-Ne laser

158   at 632 nm whose light is linearly polarized at 45°, allowing acquisition of both *p*- (light that is

159   parallel to the incident light) and *s*-polarization (light that is perpendicular to the incident light)

160   data within a single angular scan. The technique has been described previously [24, 25] (see

161   supplementary information for details).

162

163   **Formation of a planar lipid bilayer on the PWR sensor**

164   The method used to prepare the lipid bilayer is based on the procedure by Mueller and Rudin

165   [26] to make black lipid membranes (See supplementary information for details). To ensure

166   that a proper solid-supported lipid bilayer is formed, the changes in the resonance minimum

167   position (resulting from changes in mass density, anisotropy and thickness following film

168   deposition) for both polarizations are measured and compared to values previously established

169   to correspond to a lipid bilayer [27]. The lipids used for the two membrane systems studied

170   were 1-palmitoyl-2-oleoyl-sn-glycero-3-phosphocholine (POPC) and 1,2-didocosahexaenoyl-

171   sn-glycero-3-phosphocholine (DDPC).

172

173   **Immobilisation of cell fragments on the PWR sensor**

174   The protocol for adhesion of cell fragments on silica (glass slides or PWR sensor) was adapted

175   from reported work from Perez and collaborators [28] (see supplementary information for

176   details).

177

178   **Partial purification and reconstitution of the dopamine D2 receptor in the lipid bilayer**

179   D2R-expressing membranes from *Pichia pastoris* (gift from JL Banères) were used (see

180   supplementary information for details). After lipid bilayer formation, detergent-solubilized D2

181   receptor was reconstituted in the lipid bilayer by the detergent-dilution method (see

182   supplementary information for details).

183

184   **Ligand-induced receptor response**

185   Both systems (cell fragments and reconstituted protein in lipid model systems) were tested for

186   their capacity to respond to ligand to check whether the dopamine D2 receptor is active after

187   cell fragment immobilization and the reconstitution process in the lipid membrane (see

188   supplementary information for details). A control experiment was performed that consisted in

adding the same ligand concentrations to a lipid bilayer with no receptor reconstituted to measure non-specific binding of ligand to lipids alone (Fig. S4I). Graphical analysis of the spectral changes observed upon ligand addition (spectral shifts observed at maximal ligand concentration) was performed following published method [29].

cAMP accumulation assays

D2R stably expressing HEK 293 (or CHO when indicated) cells were used. The production of cAMP was measured by using a cAMP Enzyme Immunoassay kit (Sigma, CA200) as described by the manufacturer using Victor3 (Perkin Elmer) plate reader. The curve fit was obtained by GraphPad Prism 5 (GraphPad Software, Inc.) (see supplementary information for details).

Fluorescence anisotropy assay

See supplementary information for details.

β-Arrestin2 recruitment assay

β-arrestin2 recruitment was assessed using the PathHunter© express DRD2L CHO-K1 Beta arrestin GPCR Assay (DiscoverX, Fremont, CA) following the manufacturer's instructions (see supplementary information for details).

Behavioral experiments

Female C57BL6/J mice were fed with isocaloric diets containing 5% fat with a high (n-3 def diet) or low LA/ALA ratio (Ctrl diet) across gestation and lactation and offspring were maintained under the same diet after weaning as previously done (see details in [14]). All experiments were performed at adulthood (see supplementary information for details).

Operant conditioning

The apparatus and behavioral paradigms were previously described [14] (see supplementary information for details). Aripiprazole (Arip; 7-[4-[4-(2,3-dichlorophenyl)piperazin-1-yl]butoxy]-3,4-dihydro-1H-quinolin-2-one; Merck®, Darmstadt, Germany) was dissolved in a mixture of saline (NaCl 0.9%) and cremiphore (2% of cremiphore in saline) at the doses of 0.1 and 0.5 mg/kg and administered intraperitoneally 10 min before the beginning of the PRx2 test sessions as previously done (Ducrocq et al., in prep.). The ratio of lever presses under drugs

219 over lever presses after vehicle injection were measured for each animal and averaged in order
220 to evaluate the effect of the drugs on operant responding.

221 **Spontaneous locomotion**

222 Quinpirole-induced locomotor response was evaluated as described previously (Akhisaroglu
223 et al., 2005). Briefly, animals received 7 intraperitoneal injections of 1mg/kg quinpirole (Quin;
224 Tocris) dissolved in 0.9% saline every 72 hours. Locomotion was immediately measured for 3
225 hours after the 8th injection of 0.5mg/kg quinpirole (see supplementary information for details).

226 **Western blot**

227 Mice were dislocated and the brains were quickly removed, snap-frozen on dry ice and stored.
228 Nucleus accumbens samples were punched (No.18035-01, Fine Science Tools) from 200 μm
229 frozen slices in a cryostat. Samples were homogenized and denatured and western blot were
230 performed as previously described [14] (see supplementary information for details).

231 **Cell Membrane Microarray and [^{35}S]GTPγS autoradiography**

232 Microarrays were composed of a collection of membrane homogenates isolated from the NAc
233 of adult mice exposed to Ctrl diet (n=17) or n-3 def diet (n=17) and from rat cerebral cortex as
234 positive control (see supplementary information for details). Microarrays were fabricated by a
235 non-contact microarrayer (Nano_plotter NP2.1) placing the cell membrane homogenates (20
236 drops/spot) into microscope glass slides treated using a proprietary technology, which enables
237 the immobilization of cell membranes to supports preserving the structure and functionality of
238 their proteins [30].
239 [^{35}S]GTPγS binding studies were carried out using Cell Membrane Microarrays according to
240 the following protocol. Briefly, Cell Membrane Microarrays were dried 20 min at room
241 temperature (r.t.), then they were incubated in assay buffer (50 mM Tris-Cl; 1 mM EGTA; 3
242 mM MgCl$_2$; 100 mM NaCl; 0,5% BSA; pH 7,4) in the presence or absence of 50 μM GDP
243 and/or 100 μM quinpirole for 15 min at r.t.. Microarrays were transferred into assay buffer
244 containing 50 μM GDP and 0.1 nM [^{35}S]GTPγS, with and without the dopamine D2 agonist,
245 quinpirole, at 100 μM and incubated at 30°C for 30 min. Non-specific binding was determined
246 with GTPγS (10 μM). Finally, microarrays, together with [^{35}S]-standards, were exposed to films,
247 developed, scanned and quantified using the Mapix software.

248 **Lipid analyses**

249   Cells submitted to different treatments were randomly analyzed according to Joffre et al. [31].

250   Total lipids were extracted according to the method developed by Folch et al. [32] and were

251   submitted to fatty acid methylation using 7% boron trifluoride in methanol following Morrison

252   and Smith protocol [33] (see supplementary information for details).

253   **MD simulations**

254   VMD1.9.4 [34] was used to preprocess both inactive crystal (PDB ID: 6CM4) and active

255   cryoEM structures (PDB ID: 6VMS) of the dopamine D2 to set up the simulations of the apo

256   and holo states, respectively. Any co-crystallization atoms different than water molecules

257   closer than 5 Å to the protein were removed. MODELLER [35] was used to: (a) mutate back

258   to the native sequence any mutation present in the structure, namely A122I, A375L, and A379L

259   in PDB ID: 6CM4, and I205T, L222R, L374M, Y378V, L381V, and I421V in PDB ID: 6VMS,

260   and (b) model residue CYS443, which is missing in the 6CM4 structure, to have the D2R

261   palmitoylation site available. The HomolWat server [36] was used to place internal water

262   molecules not present in the initial structure, and the sodium ion in the case of apo structures.

263   An inactive apo structure was then generated by simply removing the risperidone ligand bound

264   to PDB ID: 6CM4. Likewise, an active apo structure was generated by removing the ligand

265   bromoergocryptine from PDB ID: 6VMS. This second apo structure was used to dock one

266   molecule of either dopamine or aripiprazole into the orthosteric binding pocket of the receptor

267   using AutoDock Vina [37].

268   The CHARMM-GUI builder [38, 39] was used to embed each refined structure into a 90 x 90

269   $Å^2$ multicomponent membrane rich in either DHA or DPA, using a specific and realistic lipid

270   composition [20], which is detailed in Table S2.

271   Each protein-membrane system was placed into a water box made of explicit water molecules,

272   their charge was neutralized, and the ionic strength of the system adjusted, throughout

273   CHARMM-GUI builder's pipeline. All titratable residues of the protein were left in their dominant

274   protonation state at pH 7.0, except for Asp80. Disulfide bridges were inserted between Cys107-

275   Cys182, and Cys399-Cys401, and a palmitoyl moiety was covalently linked to Cys443.

276   Systems were first energy minimized and then equilibrated for 50 ns at constant pressure (NPT

277   ensemble). The harmonic positional restraints initially applied to all Cα atoms of the protein

278   were gradually released throughout the equilibration phase. Production simulations for each

279   replica were run for 1 μs each, at constant volume (NVT ensemble), 1,013 bar and 310 K. The

280   production simulations of this study yielded an aggregated time of 16 μs (4 systems x 4 replicas

281   x 1 μs). All simulations were run using ACEMD [40] in combination with the CHARMM36m

282   force field [41]. Dopamine and aripiprazole ligand charges were optimized in the ANI-2x mode

using the parameterize module of HTMD [42]. Figures from simulations were rendered using the Tachyon renderer [43] and the R ggplot2 library [44].

Lipid-protein contact ratios between lipid species were calculated by dividing the number of contacts per atom of one lipid group over the other. Atoms closer than 4.2 Å to the center of mass of the protein were considered in contact. Only lipid tail atoms were used in these calculations. Each contact value was previously normalized by the total number of atoms in that particular selection. For example, sn-1 SDP(d)C / SAT ratios were calculated as the number of atoms of DHA < 4.2 Å of protein's center of mass divided by the total number of SDP(d)C chain atoms in the system. Likewise, SAT is calculated in the former ratio as the number of atoms of any DPPC, DSPC, or PSM chain closer than 4.2 Å of protein's center of mass divided by the total number atoms of these tails.

The average lipid occupancy across the simulations was computed using the Python package PyLipID [45]. The Jensen-Shannon distance [46] was used to compare structural ensembles from the simulations via the relative entropy analysis module of the PENSA library [47].

Statistical analyses

Data are reported as mean ± SD (unless otherwise indicated) (see supplementary information for details).

Data availability

The datasets generated and/or analyzed during the current study are available from the corresponding author on reasonable request. All MD simulation trajectories generated in this study can be visualized and inspected through the GPCRmd online resource [48].

Results

1. **Membrane n-3 PUFAs, but not n-6 PUFAs, modulate the binding affinity of D2R ligands**

To determine the impact of membrane lipid unsaturation on D2R ligand binding, HEK cells were incubated with PUFAs, which is known to result in their esterification into the *sn*-2 position of phospholipids [49]. We used two different PUFAs, the n-3 PUFA DHA (C22:6) and the n-6 PUFA DPA (C22:5), which display the same carbon chain length, but differ in one double bond. A lipid analysis confirmed the enrichment of phospholipids in DHA or DPA and monitored its efficient incorporation in cell membranes, leading to a comparable proportion of either PUFA after treatment (Fig. S1). We measured the binding affinity of D2R ligands on supported cell

membranes expressing the D2R using plasmon waveguide resonance (PWR) spectroscopy [50]. Membrane enrichment in DHA, but not DPA, significantly enhanced ligand binding affinities, for agonists (quinpirole and dopamine), antagonist (spiperone), and partial agonist (aripiprazole) (Fig. 1A). Thus, dissociation constants (K_D) calculated from resonance position shifts followed in p- and s-polarization upon incremental addition of ligands were decreased across all D2R ligands tested under DHA membrane enrichment (Fig. 1A-B). K_D values correspond to the average between p- and s-data and are comparable to the ones reported in the literature, which validates our system and confirms that the receptor maintains functionality in these conditions (Fig. S2) [51, 52]. We further confirmed the potentiating effect of membrane DHA enrichment on D2R ligand binding affinity for the spiperone-derived fluorescent ligand NAPS-d2 through fluorescence anisotropy in cell membrane fragments [53, 54] (Fig. S3) and PWR with partially purified D2R reconstituted in model membranes of pure POPC (16:0 / 18:1) and pure DDPC (22:6 / 22:6) (Fig. S4). Of note, ligand addition to cell membrane fragments not expressing the D2R resulted in negligible spectral changes (Fig. S4). Therefore, spectral changes observed upon ligand binding with D2R expression are mainly due to receptor conformational changes and accompanying lipid reorganization.

Graphical analysis of the spectral changes allowed determination of the contribution of mass and structural changes. Overall, the data indicate that spectral changes are a result of both mass and structural changes with mass changes predominating (Fig. S4J). Interestingly, we observed that both agonist and antagonist lead to different polarization responses that were positive both for agonists (quinpirole, dopamine) and partial agonist (aripiprazole), and negative for the antagonist spiperone (Fig. 1B-D and Fig. S2). These results show that different classes of ligands induce distinct conformational changes upon binding to the D2R, as previously reported for other GPCRs [24, 55–58]. Importantly, the receptor conformational changes became less anisotropic for dopamine and more anisotropic for aripiprazole (as shown by the respective decrease and increase in p-polarization shifts; Fig. 1B). Overall, the presence of membrane PUFAs significantly influence changes in receptor's conformation induced by ligands along the receptor long axis (p-polarization) (Fig. 1C-D).

2. MD simulations reveal that n-3 and n-6 PUFAs differentially interact with the D2R

With the aim of gaining structural insights into the differential modulation exerted by DPA and DHA in PUFA-enriched cell membranes, we used MD simulations to study the interaction between the D2R and membranes enriched in either DHA or DPA. We first simulated four

351 replicas of the D2R embedded in a multicomponent membrane (see Methods) enriched in

352 either DHA-containing phospholipids (1-stearoyl-2-docosahexaenoyl-sn-glycero-3-

353 phosphocholine, SD(h)PC) or DPA-containing phospholipids (1-stearoyl-2-

354 docosa(p)entaenoyl-sn-glycero-3-phosphocholine, SD(p)PC). In line with previous reports,

355 [20, 21], SD(h)PC tends to displace saturated phospholipids from the membrane "solvation"

356 shell that surrounds the D2R, due to the much higher propensity of DHA tails for the interaction

357 with the receptor (Fig. S5). Strikingly, the loss of just one double bond (i.e. replacing DHA by

358 DPA) abolishes this propensity, as shown by the much lower interaction ratio of SD(p)PC

359 molecules with the receptor during the simulation (Fig. S5). Specifically, the propensity for the

360 interaction with the D2R is three-fold higher for DHA tails (Table 1).

361

362 Moreover, our simulations show that DHA and DPA display a different pattern of interaction

363 with the receptor (Fig. 2A). Interestingly, SD(p)PC lipid molecules display a clear preference

364 over SD(h)PC for interaction with the extracellular segments of transmembrane helix (TM) 1,

365 TM2, and TM7(Fig. 2B, bottom left).

366

367 We then simulated the D2R bound to dopamine or aripiprazole, and embedded into a

368 multicomponent membrane enriched in SD(h)PC (see Methods). Interestingly, while the

369 aripiprazole-bound D2R simulations also showed an increased level of DHA around the

370 receptor (Fig. 2C), the DHA solvation effect was absent or even diminished in dopamine-bound

371 D2R simulations (Fig. 2C). Specifically, the propensity for the interaction between DHA tails

372 and the protein was approximately two-fold higher in the aripiprazole-bound compared to

373 unbound D2R simulations (Table 2). Furthermore, as shown in Fig. 2D, the presence of

374 dopamine or aripiprazole in the binding pocket induced different patterns of interactions

375 between SD(h)PC and the D2R, including a different interaction signature at the extracellular

376 segment of the receptor where ligand binds (Fig. 2D, upper left and right panels).

377

378 Lastly, we investigated the effect of DHA vs DPA on the conformational dynamics of the D2R.

379 To find D2R structural differences between DHA-rich and DPA-rich simulations, we used a

380 relative entropy analysis (see Methods) to compare the conformational ensemble of the

381 receptor across all replicas. As shown in Fig. 2E, DHA- and DPA-rich systems induce very

382 similar conformational dynamics of the D2R. To investigate whether decreasing the amount of

383 membrane PUFAs has an effect on the conformational dynamics of the receptor, we simulated

384 four replicas of the D2R embedded into a multicomponent membrane depleted of SD(h)PC

385 (see Methods). The relative entropy analysis revealed that a decrease in PUFAs has a strong

386 effect on D2R's conformational dynamics. As shown in Fig. 2F-H, most of these differences

387 are at the level of D2R intra- and extracellular loops, likely due to a different hydrophobic

mismatch between the receptor and the lipid bilayer. Interestingly, despite being relatively short, the intracellular loop 2 (ICL2) of the receptor displays completely different dynamics under PUFA depletion. A visual inspection of the simulations showed that PUFA-rich membranes preserve the helicity of the intracellular end of helix 4, whereas this segment of the receptor is completely unfolded in PUFA-depleted membranes. Specifically, helix 4 losses more than one helix turn at the level of residues 146 - 150 (Fig. 2I-J). These figures clearly show that the loss of this turn particularly affects the position of two consecutive serine residues in helix 4, namely S147 and S148, leading to rearrangement of ICL2.

3. n-3 and n-6 PUFAs do not influence the D_2R $G_{\alpha i/o}$-mediated signaling pathway but enhance maximal recruitment of β-arrestin2

In order to evaluate the downstream effect of PUFAs, we performed dose-response experiments where we probed the signaling efficacy of the D2R in the presence and absence of PUFAs in heterologous systems. First, we treated cells with 10 µM PUFAs (Fig. S6) and measured the inhibition of forskolin-induced cAMP production upon treatment with quinpirole, dopamine and aripiprazole as a proxy for $G_{i/o}$ protein activation. As shown in Fig. S7A and Table S1, both control and PUFA-rich cells display a similar agonist-dependent decrease in cAMP production, which suggests that PUFAs do not modulate the $G_{i/o}$ protein signaling pathway. Next, we used the same experimental conditions to study the $G_{i/o}$ protein-independent signaling pathway by measuring β-arrestin2 recruitment. In these experiments, while PUFAs did not affect the potency of β-arrestin2 recruitment (i.e. EC_{50}), they slightly (quinpirole and dopamine) affected its efficacy (i.e. E_{max}) (Fig. S7D-F). To confirm this trend, we treated cells with a higher amount of PUFAs (i.e. 30 µM) (Fig. S6). We did not observe any impact of PUFAs enrichment on basal cAMP production (Fig. S7B). We then performed dose-response experiments upon ligand stimulation. Higher PUFA manipulations did not influence cAMP production in two cell lines (Fig. 3A, C, E and Fig. S7C), or the EC_{50} for β-arrestin2 recruitment, but significantly increased the E_{max} of β-arrestin2 recruitment for all ligands in both DHA- and DPA-rich cells (Fig. 3B, D, F).

Altogether, our data reveal that membrane unsaturation with either DPA or DHA enrichment does not affect $G_{i/o}$ protein activation but enhances β-arrestin2 recruitment efficacy.

4. Decreased unsaturation by n-3 PUFA deficiency blunts D2R ligand-induced alterations in locomotion and motivation

423   To translate our *in vitro* findings to *in vivo* settings, we used a validated model of n-3 PUFA

424   deficiency in mice in which we demonstrated a dysfunction of D2R-expressing neurons [14].

425   We previously showed that, in the brain of n-3 PUFA deficient mice, DHA is replaced by DPA,

426   mostly in phosphoethanolamine (PE) species [14]. We calculated an unsaturation index [59,

427   60] and found that n-3 PUFA deficiency leads to decreased unsaturation within PEs (Fig S8A-

428   C).

429   Using striatal extracts – in which D2R is highly expressed – we found that i) Gi protein

430   recruitment in response to quinpirole application is unaffected (Fig. 4A) and ii) phosphorylation

431   of the glycogen synthase kinase β (GSK3β), a key signaling enzyme downstream of β-arrestin2

432   [61], is decreased at basal states in n-3 PUFA deficient animals (Fig. 4B and Fig. S9). These

433   latter findings are consistent with our *in vitro* data showing that membrane PUFA enrichment

434   potentiates the recruitment of β-arrestin2 at the D2R. Next, we used n-3 PUFA deficient

435   animals to study behavioral responses to D2R ligands. Our results show that n-3 PUFA

436   deficient animals display decreased locomotor response under quinpirole administration (Fig.

437   4C). Finally, we found that peripheral administration of aripiprazole blunted performance in an

438   operant conditioning-based motivational task in control animals, while n-3 PUFA deficient mice

439   were partially insensitive to aripiprazole (Fig. 4D).

440

441   **Discussion**

442   While most early reports on the preferential interaction between PUFAs and GPCRs focused

443   on the interaction of rhodopsin with DHA [15–19], recent studies have confirmed that PUFAs

444   can also modulate the activity and function of other GPCRs including the cannabinoid CB1

445   receptor [62], the D2R [20, 21] and the adenosine A2A receptor [20, 21, 63]. Here, we focus

446   on the interplay of PUFAs with the D2R, considering the relevance of this receptor to the

447   pathophysiology of neuropsychiatric disorders and their pharmacological treatments. We found

448   that DHA- but not DPA-rich phospholipids potentiate the binding affinity of both agonists and

449   antagonists for the D2R. In line with this finding, MD simulations show a preferential interaction

450   of the D2R with DHA tails compared to DPA tails. Both DHA and DPA seem to induce very

451   similar conformational dynamics on the D2R and relative entropy analyses showed that the

452   presence of PUFAs in the membrane selectively affects the conformation of ICL2. At the

453   signaling level, both DPA and DHA enhance β-arrestin2 recruitment efficacy without affecting

454    $G_{i/o}$ protein activity. Finally, we show that n-3 deficient animal models, in which membrane

455   unsaturation is lower, display altered behavioral responses upon treatment with D2R ligands.

456

457   Our findings clearly show that DHA, but not DPA, enhances D2R ligand binding, suggesting

458   that DHA acts as an allosteric modulator of the receptor. Various studies demonstrate that

459 PUFAs tend to preferentially interact with GPCRs [18, 19, 64, 65] and our MD simulations
460 confirm that DHA – but not DPA – tails preferentially interact with the D2R when compared to
461 saturated ones, as previously reported [20, 21]. In addition, we found that DHA- and DPA-
462 containing phospholipids differentially interact with extracellular segments of transmembrane
463 helix (TM) 1, TM2, and TM7, which define entry crevices for water and phospholipid
464 headgroups into the binding pocket [66]. These findings suggest that direct interactions with
465 the receptor could partly mediate the effect of DHA on D2R ligand binding. PUFA-containing
466 phospholipids can also exert a strong influence on the physical and mechanical properties of
467 biological membranes including thickness, bending or rigidity [67] and, hence, subtle changes
468 in these properties can indirectly modulate the function of transmembrane proteins [67–69].
469 Therefore, PUFA-rich membranes could potentially favor specific conformations of the D2R to
470 modulate its ligand binding affinity. In particular, n-3 PUFAs provide transmembrane proteins
471 with a flexible environment that enables such modulation [69–71]. Despite differing in just one
472 double bond, n-6 PUFAs do not seem to increase membrane elasticity to the same extent [72],
473 which could also account for the differential effects of DHA and DPA on D2R ligand-binding
474 affinity. Furthermore, by increasing membrane fluidity and/or packing defects [8], n-3 PUFAs
475 could alter the accessibility of ligand into the D2R or its exit from the binding site, thereby
476 modulating ligand binding affinity. In fact, most antipsychotics (i.e. D2R ligands) display high
477 membrane partitioning properties [73, 74]. Of note, Lolicato et al. recently suggested that the
478 entry pathway of dopamine into the D2R likely requires this neurotransmitter to first partition
479 into the membrane [75].
480
481 Intriguingly, our simulations show that the preferential interaction of DHA with the D2R is lower
482 or completely absent in the presence of ligands in the binding pocket. This result suggests a
483 scenario where the conformational state induced by the ligand could also modulate the
484 interaction propensity between the membrane and the receptor, as recently suggested for
485 cholesterol and the oxytocin receptor [76]. While further investigation will be needed to unravel
486 the precise molecular mechanisms behind the effect of DHA on ligand binding affinity, our work
487 suggests that DHA can act as an allosteric modulator of the D2R, both by influencing the bulk
488 membrane properties and by establishing direct interactions with the receptor.
489
490 Our dose-response experiments in cells show that the selective enhancing effect of DHA on
491 D2R ligand binding affinity does not correlate with enhanced potency of relevant downstream
492 protein effectors. Membrane PUFA enrichment does not alter the potency or efficacy of D2R
493 agonists inhibiting cAMP production supporting a lack of effect on $G_{i/o}$ protein signaling,
494 consistent with previous reports [77–79]. Similarly, there was no effect of DPA or DHA on the
495 potency (EC_{50}) of agonist-induced β-arrestin recruitment, despite an enhancement of maximal

efficacy (E_{max}). These data suggest that the effects of PUFAs on D2R signaling are at least partially uncoupled from the changes in receptor binding properties. One possibility is that the relatively small changes in ligand binding affinity induced by PUFAs on ligand binding affinity might be difficult to detect using signalling assays in heterologous system. Alternatively, while highly speculative, our findings are in line with the emerging notion of "loose allosteric coupling", which implies that conformational changes in the binding pocket region facilitate, but do not necessarily dictate specific conformations at the intracellular end of the receptor [80, 81].

Our findings consistently show that both DHA and DPA enhance the maximal efficacy of β-arrestin2 recruitment. This is compatible with the fact that PUFAs can alter the lateral organization of membranes [49, 82–84] and change the domain partitioning properties of GPCRs including the D2R [20, 21]. As previously suggested [85–90], altering receptor partitioning could modulate recruitment of GRKs and receptor phosphorylation and, in turn, influence β-arrestin coupling. It is also worth speculating that PUFA-induced membrane packing defects [8] could alter β-arrestin recruitment by modulating the membrane anchoring of its C-edge loops [91]. Interestingly, our MD simulations show that the presence of membrane PUFAs influence the conformational dynamics of the D2R, especially within a protein segment of the ICL2 that encompasses two consecutive serine residues – S147 and S148. These residues are involved in D2R phosphorylation [92] and located just upstream of Lysine 149, an important residue for β-arrestin binding at the D2R [93]. Considering the important role of ICL2 in the recruitment of β-arrestin by the D2R [94], the effect of membrane unsaturation on the structure of this loop could therefore be one key mechanism underlying enhancement of β-arrestin2 recruitment by PUFAs.

Overall, our *in vitro* and *in silico* findings show that membrane unsaturation can influence the activity of the D2R in at least two partially distinct ways, i) changes in ligand binding affinity which seems to be specific to DHA, and ii) recruitment of β-arrestin signaling. These effects may have important physiological impact in the context of chronic alterations in PUFA levels, in particular when occurring during brain development. This hypothesis is supported by our *in vivo* findings in a model of chronic deficiency in n-3 PUFAs [14] that results in a decrease of overall membrane unsaturation. In fact, in accordance with our *in vitro* results, while n-3 PUFA deficiency does not seem to affect D2R-mediated activation of the $G_{i/o}$ protein in the striatum, the decrease in phospho-GSK3 expression is consistent with an impairment of β-arrestin2-dependent signaling, since GSK3 phosphorylation is reduced by β-arrestin2 recruitment to the D2R [61]. Notably, D2R-mediated locomotor response has recently been shown to also

532 depend on β-arrestin2-, but not $G_{i/o}$ protein-, mediated signalling [95]. In line with this, we find
533 that D2R agonist (quinpirole)-induced increase in locomotion is blunted in n-3 PUFA deficient
534 animals, consistent with an impairment in β-arrestin2 recruitment and downstream signalling.
535 However, we find that aripiprazole-induced decrease in motivation – which might result from
536 an antagonistic activity of aripiprazole at the D2R - is also blunted in n-3 PUFA deficient
537 animals. D2R-mediated modulation of motivation has been shown to be independent of β-
538 arrestin2-dependent signalling [95], but rather to rely on $G_{i/o}$ protein-mediated transmission at
539 synaptic terminals in the ventral pallidum [96]. This raises the intriguing hypothesis that
540 membrane PUFAs could differentially modulate D2R signalling activity in distinct neuronal
541 subcompartments. Even though further work will be needed to disentangle the precise
542 mechanisms by which PUFAs modulate D2R activity *in vivo*, these latter data are in line with
543 the recent demonstration that motivational deficits in n-3 PUFA deficient animals directly
544 relates to a dysfunction of D2R-expressing neurons [14].

545

546 Uncovering the precise mechanisms by which brain PUFA biostatus influences D2R-
547 dependent signalling and downstream-related behaviors will require further work. Nonetheless,
548 taken together, our results show that n-3 PUFAs can act as allosteric modulators of the D2R
549 and potentiate its signalling activity, in particular the β-arrestin2 component. This raises the
550 intriguing hypothesis that n-3 PUFA supplementation could alter the effects of D2R ligands,
551 including antipsychotics. In accordance with this idea, several clinical trials have shown that n-
552 3 PUFA supplementation accelerates treatment response, improves the tolerability of
553 antipsychotics in first-episode psychoses [97, 98], and reduces prescription rate of
554 antipsychotics [99]. Our data suggest that direct action of PUFA membrane composition on
555 D2R activity could mediate such effects.

556

Author contributions

M-L.J, V.D.P, R.G-G, I.D.A. and P.T. conceived and supervised the study. J.S., G.B-G., E.M., T.D. and J.A.J. provided expertise, reagents and supervised specific experiments. M-L.J., V.D.P., F.D., A.O., R.B., M-F.A., M.H.P., B.M-L., J.S., S.M., S.V., T.T-C., S.G. and R.G-G performed experiments and analyzed the data. M-L.J., V.D.P., R.G.-G., I.D.A. and P.T. wrote the original version of the manuscript. All authors discussed the results and reviewed the manuscript.

Conflict of Interest

The authors declare no competing financial interests.

References

1.   Rohrbough J, Broadie K. Lipid regulation of the synaptic vesicle cycle. Nat Rev Neurosci. 2005;6:139–150.

2.   Bazinet RP, Layé S. Polyunsaturated fatty acids and their metabolites in brain function and disease. Nat Rev Neurosci. 2014;15:771–785.

3.   Messamore E, McNamara RK. Detection and treatment of omega-3 fatty acid deficiency in psychiatric practice: Rationale and implementation. Lipids Health Dis. 2016;15:1–13.

4.   Ohi K, Ursini G, Li M, Shin JH, Ye T, Chen Q, et al. DEGS2 polymorphism associated with cognition in schizophrenia is associated with gene expression in brain. Transl Psychiatry. 2015;5:1–6.

5.   Shimamoto C, Ohnishi T, Maekawa M, Watanabe A, Ohba H, Arai R, et al. Functional characterization of FABP3, 5 and 7 gene variants identified in schizophrenia and autism spectrum disorder and mouse behavioral studies. Hum Mol Genet. 2014;23:6495–6511.

600   6.   Beltz BS, Tlusty MF, Benton JL, Sandeman DC. Omega-3 fatty acids upregulate adult
601   neurogenesis. Neurosci Lett. 2007;415:154–158.

602   7.   Calderon F, Kim HY. Docosahexaenoic acid promotes neurite growth in hippocampal
603   neurons. J Neurochem. 2004;90:979–988.

604   8.   Harayama T, Riezman H. Understanding the diversity of membrane lipid composition.
605   Nat Rev Mol Cell Biol. 2018;19:281–296.

606   9.   Dawaliby R, Trubbia C, Delporte C, Masureel M, Van Antwerpen P, Kobilka BK, et al.
607   Allosteric regulation of G protein-coupled receptor activity by phospholipids. Nat Chem
608   Biol. 2016;12:35–39.

609   10. Duncan AL, Song W, Sansom MSP. Lipid-dependent regulation of ion channels and g
610   protein-coupled receptors: Insights from structures and simulations. Annu Rev
611   Pharmacol Toxicol. 2020;60:31–50.

612   11. Whitton AE, Treadway MT, Pizzagalli DA. Reward processing dysfunction in major
613   depression, bipolar disorder and schizophrenia. Curr Opin Psychiatry. 2015;28:7–12.

614   12. Bondi CO, Taha AY, Tock JL, Totah NKB, Cheon Y, Torres GE, et al. Adolescent
615   behavior and dopamine availability are uniquely sensitive to dietary omega-3 fatty acid
616   deficiency. Biol Psychiatry. 2014;75:38–46.

617   13. Chalon S. Omega-3 fatty acids and monoamine neurotransmission. Prostaglandins
618   Leukot Essent Fat Acids. 2006;75:259–269.

619   14. Ducrocq F, Walle R, Contini A, Oummadi A, Caraballo B, van der Veldt S, et al.
620   Causal Link between n-3 Polyunsaturated Fatty Acid Deficiency and Motivation
621   Deficits. Cell Metab. 2020;31:755–772.

622   15. Litman BJ, Mitchell DC. A role for phospholipid polyunsaturation in modulating
623   membrane protein function. Lipids. 1996;31:193–197.

624   16. Mitchell DC, Niu SL, Litman BJ. Enhancement of G protein-coupled signaling by DHA
625   phospholipids. Lipids. 2003;38:437–443.

626   17. Salem N, Litman B, Kim H, Gawrisch K. Mechanisms of Action of Docosahexaenoic
627   Acid in the Nervous System. Lipids. 2001;36:945–959.

628   18. Feller SE, Gawrisch K, Woolf TB. Rhodopsin exhibits a preference for solvation by
629   polyunsaturated docosohexaenoic acid. J Am Chem Soc. 2003;125:4434–4435.

630   19. Pitman MC, Grossfield A, Suits F, Feller SE. Role of cholesterol and polyunsaturated
631   chains in lipid-protein interactions: Molecular dynamics simulation of rhodopsin in a
632   realistic membrane environment. J Am Chem Soc. 2005;127:4576–4577.

633   20. Guixà-González R, Javanainen M, Gómez-Soler M, Cordobilla B, Domingo JC, Sanz
634   F, et al. Membrane omega-3 fatty acids modulate the oligomerisation kinetics of
635   adenosine A2A and dopamine D2 receptors. Sci Rep. 2016;6:1–13.

636   21. Javanainen M, Enkavi G, Guixà-Gonzaléz R, Kulig W, Martinez-Seara H, Levental I, et

637 al. Reduced level of docosahexaenoic acid shifts GPCR neuroreceptors to less
638 ordered membrane regions. PLoS Comput Biol. 2019;15:1–16.

639 22. Polozova A, Litman BJ. Cholesterol dependent recruitment of di22:6-PC by a G
640 protein-coupled receptor into lateral domains. Biophys J. 2000;79:2632–2643.

641 23. De Smedt-Peyrusse V, Sargueil F, Moranis A, Harizi H, Mongrand S, Layé S.
642 Docosahexaenoic acid prevents lipopolysaccharide-induced cytokine production in
643 microglial cells by inhibiting lipopolysaccharide receptor presentation but not its
644 membrane subdomain localization. J Neurochem. 2008;105:296–307.

645 24. Alves ID, Lecomte S. Study of G-Protein Coupled Receptor Signaling in Membrane
646 Environment by Plasmon Waveguide Resonance. Acc Chem Res. 2019;52:1059–
647 1067.

648 25. Salamon Z, Macleod HA, Tollin G. Coupled plasmon-waveguide resonators: A new
649 spectroscopic tool for probing proteolipid film structure and properties. Biophys J.
650 1997;73:2791–2797.

651 26. Mueller P, Rudin DO. Resting and action potentials in experimental bimolecular lipid
652 membranes. J Theor Biol. 1968;18:222–258.

653 27. Harté E, Maalouli N, Shalabney A, Texier E, Berthelot K, Lecomte S, et al. Probing the
654 kinetics of lipid membrane formation and the interaction of a nontoxic and a toxic
655 amyloid with plasmon waveguide resonance. Chem Commun. 2014;50:4168–4171.

656 28. Perez JB, Segura JM, Abankwa D, Piguet J, Martinez KL, Vogel H. Monitoring the
657 Diffusion of Single Heterotrimeric G Proteins in Supported Cell-membrane Sheets
658 Reveals their Partitioning into Microdomains. J Mol Biol. 2006;363:918–930.

659 29. Salamon Z, Tollin G. Graphical Analysis of Mass and Anisotropy Changes Observed
660 by Plasmon-Waveguide Resonance Spectroscopy Can Provide Useful Insights into
661 Membrane Protein Function. Biophys J. 2004;86:2508–2516.

662 30. Fernández R, Garate J, Tolentino-Cortez T, Herraiz A, Lombardero L, Ducrocq F, et
663 al. Microarray and Mass Spectrometry-Based Methodology for Lipid Profiling of
664 Tissues and Cell Cultures. Anal Chem. 2019;91:15967–15973.

665 31. Joffre C, Grégoire S, De Smedt V, Acar N, Bretillon L, Nadjar A, et al. Modulation of
666 brain PUFA content in different experimental models of mice. Prostaglandins Leukot
667 Essent Fat Acids. 2016;114:1–10.

668 32. Folch J, Lees M, Sloane Stanley GH. A simple method for the isolation and purification
669 of total lipides from animal tissues. J Biol Chem. 1957;226:497–509.

670 33. Morrison WR, Smith LM. Preparation of fatty acid methyl esters and dimethylacetals
671 from lipids. J Lipid Res. 1964;5:600–608.

672 34. Humphrey W, Dalke A, Schulten K. VMD: Visual molecular dynamics. J Mol Graph.
673 1996;14:33–38.

674   35.   Webb B, Sali A. Comparative Protein Structure Modeling Using MODELLER. Curr
675   Protoc Bioinforma. 2016;54:5.6.1-5.6.37.

676   36.   Mayol E, Garcia-Recio A, Tiemann JKS, Hildebrand PW, Guixa-Gonzalez R, Olivella
677   M, et al. Homolwat: A web server tool to incorporate 'homologous' water molecules
678   into gpcr structures. Nucleic Acids Res. 2020;48:W54–W59.

679   37.   Trott O, Olson AJ. AutoDock Vina: Improving the speed and accuracy of docking with
680   a new scoring function, efficient optimization, and multithreading. J Comput Chem.
681   2009;31.

682   38.   Jo S, Kim T, Im W. Automated builder and database of protein/membrane complexes
683   for molecular dynamics simulations. PLoS One. 2007;2:e880.

684   39.   Wu EL, Cheng X, Jo S, Rui H, Song KC, Dávila-Contreras EM, et al. CHARMM-GUI
685   membrane builder toward realistic biological membrane simulations. J Comput Chem.
686   2014;35:1997–2004.

687   40.   Harvey MJ, Giupponi G, De Fabritiis G. ACEMD: Accelerating biomolecular dynamics
688   in the microsecond time scale. J Chem Theory Comput. 2009;5:1632–1639.

689   41.   Huang J, Rauscher S, Nawrocki G, Ran T, Feig M, De Groot BL, et al. CHARMM36m:
690   An improved force field for folded and intrinsically disordered proteins. Nat Methods.
691   2016;14:71–73.

692   42.   Doerr S, Harvey MJ, Noé F, De Fabritiis G. HTMD: High-Throughput Molecular
693   Dynamics for Molecular Discovery. J Chem Theory Comput. 2016;12:1845–1852.

694   43.   Stone JE, Vandivort KL, Schulten K. GPU-accelerated molecular visualization on
695   petascale supercomputing platforms. Proc. UltraVis 2013 8th Int. Work. Ultrascale Vis.
696   - Held Conjunction with SC 2013 Int. Conf. High Perform. Comput. Networking,
697   Storage Anal., 2013.

698   44.   Wickham H. Ggplot2: Elegant Graphics for Data Analysis. Springer, 2016.

699   45.   Song W, Corey RA, Ansell TB, Cassidy CK, Horrell MR, Duncan AL, et al. PyLipID: A
700   Python Package for Analysis of Protein−Lipid Interactions from Molecular Dynamics
701   Simulations. J Chem Theory Comput. 2022;18:31.

702   46.   Lin J. Divergence Measures Based on the Shannon Entropy. IEEE Trans Inf Theory.
703   1991;37:145–151.

704   47.   Martin Vögele. PENSA (0.1.2). Zenodo. 2021. 2021.

705   48.   Rodríguez-Espigares I, Torrens-Fontanals M, Tiemann JKS, Aranda-García D,
706   Ramírez-Anguita JM, Stepniewski TM, et al. GPCRmd uncovers the dynamics of the
707   3D-GPCRome. Nat Methods. 2020;17:777–787.

708   49.   Stillwell W, Wassall SR. Docosahexaenoic acid: membrane properties of a unique
709   fatty acid. Chem Phys Lipids. 2003;126:1–27.

710   50.   Alves I, Park C, Hruby V. Plasmon Resonance Methods in GPCR Signaling and Other

711   Membrane Events. Curr Protein Pept Sci. 2005;6:293–312.

712 51. De Jong LAA, Grünewald S, Franke JP, Uges DRA, Bischoff R. Purification and

713   characterization of the recombinant human dopamine D2S receptor from Pichia

714   pastoris. Protein Expr Purif. 2004;33:176–184.

715 52. Malmberg A, Mohell N. Characterization of [3H]quinpirole binding to human dopamine

716   D(2A) and D3 receptors: Effects of ions and guanine nucleotides. J Pharmacol Exp

717   Ther. 1995;274:790–797.

718 53. Albizu L, Cottet M, Kralikova M, Stoev S, Seyer R, Brabet I, et al. Time-resolved FRET

719   between GPCR ligands reveals oligomers in native tissues. Nat Chem Biol.

720   2010;6:587–594.

721 54. Maurel D, Comps-Agrar L, Brock C, Rives ML, Bourrier E, Ayoub MA, et al. Cell-

722   surface protein-protein interaction analysis with time-resolved FRET and snap-tag

723   technologies: Application to GPCR oligomerization. Nat Methods. 2008;5:561–567.

724 55. Alves ID, Cowell SM, Salamon Z, Devanathan S, Tollin G, Hruby VJ. Different

725   structural states of the proteolipid membrane are produced by ligand binding to the

726   human δ-opioid receptor as shown by plasmon-waveguide resonance spectroscopy.

727   Mol Pharmacol. 2004;69:1248–1257.

728 56. Alves ID, Delaroche D, Mouillac B, Salamon Z, Tollin G, Hruby VJ, et al. The two NK-1

729   binding sites correspond to distinct, independent, and non-interconvertible receptor

730   conformational states as confirmed by plasmon-waveguide resonance spectroscopy.

731   Biochemistry. 2006;45:5309–5318.

732 57. Boyé K, Pujol N, D Alves I, Chen YP, Daubon T, Lee YZ, et al. The role of

733   CXCR3/LRP1 cross-talk in the invasion of primary brain tumors. Nat Commun.

734   2017;8:1–20.

735 58. Boyé K, Billottet C, Pujol N, Alves ID, Bikfalvi A. Ligand activation induces different

736   conformational changes in CXCR3 receptor isoforms as evidenced by plasmon

737   waveguide resonance (PWR). Sci Rep. 2017;7:1–11.

738 59. Lee J, Welti R, Roth M, Schapaugh WT, Li J, Trick HN. Enhanced seed viability and

739   lipid compositional changes during natural ageing by suppressing phospholipase Dα in

740   soybean seed. Plant Biotechnol J. 2012;10:164–173.

741 60. Takahashi D, Imai H, Kawamura Y, Uemura M. Lipid profiles of detergent resistant

742   fractions of the plasma membrane in oat and rye in association with cold acclimation

743   and freezing tolerance. Cryobiology. 2016;72:123–134.

744 61. Beaulieu JM, Gainetdinov RR, Caron MG. The Akt-GSK-3 signaling cascade in the

745   actions of dopamine. Trends Pharmacol Sci. 2007;28:166–172.

746 62. Lafourcade M, Larrieu T, Mato S, Duffaud A, Sepers M, Matias I, et al. Nutritional

747   omega-3 deficiency abolishes endocannabinoid-mediated neuronal functions. Nat

748   Neurosci. 2011;14:345–350.

749 63.   Mizumura T, Kondo K, Kurita M, Kofuku Y, Natsume M, Imai S, et al. Activation of

750   adenosine A2A receptor by lipids from docosahexaenoic acid revealed by NMR. Sci

751   Adv. 2020;6:8544–8562.

752 64.   Grossfield A, Feller SE, Pitman MC. A role for interactions in the modulation of

753   rhodopsin by ω-3 polyunsaturated lipids. Proc Natl Acad Sci U S A. 2006;103:4888–

754   4893.

755 65.   Soubias O, Teague WE, Gawrisch K. Evidence for specificity in lipid-rhodopsin

756   interactions. J Biol Chem. 2006;281:33233–33241.

757 66.   Guixà-González R, Albasanz JL, Rodriguez-Espigares I, Pastor M, Sanz F, Martí-

758   Solano M, et al. Membrane cholesterol access into a G-protein-coupled receptor. Nat

759   Commun. 2017;8:1–12.

760 67.   Carrillo-Tripp M, Feller SE. Evidence for a mechanism by which ω-3 polyunsaturated

761   lipids may affect membrane protein function. Biochemistry. 2005;44:10164–10169.

762 68.   Bruno MJ, Koeppe RE, Andersen OS. Docosahexaenoic acid alters bilayer elastic

763   properties. Proc Natl Acad Sci U S A. 2007;104:9638–9643.

764 69.   Caires R, Sierra-Valdez FJ, Millet JRM, Herwig JD, Roan E, Vásquez V, et al. Omega-

765   3 Fatty Acids Modulate TRPV4 Function through Plasma Membrane Remodeling. Cell

766   Rep. 2017;21:246–258.

767 70.   Antonny B, Vanni S, Shindou H, Ferreira T. From zero to six double bonds:

768   Phospholipid unsaturation and organelle function. Trends Cell Biol. 2015;25:427–436.

769 71.   Gawrisch K, Eldho N V., Holte LL. The structure of DHA in phospholipid membranes.

770   Lipids. 2003;38:445–452.

771 72.   Jacobs ML, Faizi HA, Peruzzi JA, Vlahovska PM, Kamat NP. EPA and DHA

772   differentially modulate membrane elasticity in the presence of cholesterol. Biophys J.

773   2021;120:2317–2329.

774 73.   Alves I, Staneva G, Tessier C, Salgado GF, Nuss P. The interaction of antipsychotic

775   drugs with lipids and subsequent lipid reorganization investigated using biophysical

776   methods. Biochim Biophys Acta - Biomembr. 2011;1808:2009–2018.

777 74.   Tessier C, Nuss P, Staneva G, Wolf C. Modification of membrane heterogeneity by

778   antipsychotic drugs: An X-ray diffraction comparative study. J Colloid Interface Sci.

779   2008;320:469–475.

780 75.   Lolicato F, Juhola H, Zak A, Postila PA, Saukko A, Rissanen S, et al. Membrane-

781   Dependent Binding and Entry Mechanism of Dopamine into Its Receptor. ACS Chem

782   Neurosci. 2020;11:1914–1924.

783 76.   Lemel L, Nieścierowicz K, García-Fernández MD, Darré L, Durroux T, Busnelli M, et

784   al. The ligand-bound state of a G protein-coupled receptor stabilizes the interaction of

785   functional cholesterol molecules. J Lipid Res. 2021;62:1–17.

786   77.   Malnoe A, Milon H, Reme C. Effect of In Vivo Modulation of Membrane
787   Docosahexaenoic Acid Levels on the Dopamine-Dependent Adenylate Cyclase
788   Activity in the Rat Retina. J Neurochem. 1990;55:1480–1485.

789   78.   Murphy MG. Effects of exogenous linoleic acid on fatty acid composition, receptor-
790   mediated cAMP formation, and transport functions in rat astrocytes in primary culture.
791   Neurochem Res. 1995;20:1365–1375.

792   79.   Yu JZ, Wang J, Sheridan SD, Perlis RH, Rasenick MM. N-3 polyunsaturated fatty
793   acids promote astrocyte differentiation and neurotrophin production independent of
794   cAMP in patient-derived neural stem cells. Mol Psychiatry. 2021;26:4605–4615.

795   80.   Latorraca NR, Venkatakrishnan AJ, Dror RO. GPCR dynamics: Structures in motion.
796   Chem Rev. 2017;117:139–155.

797   81.   Weis WI, Kobilka BK. The Molecular Basis of G Protein-Coupled Receptor Activation.
798   Annu Rev Biochem. 2018;87:897–919.

799   82.   Chapkin RS, Wang N, Fan YY, Lupton JR, Prior IA. Docosahexaenoic acid alters the
800   size and distribution of cell surface microdomains. Biochim Biophys Acta - Biomembr.
801   2008;1778:466–471.

802   83.   Levental KR, Lorent JH, Lin X, Skinkle AD, Surma MA, Stockenbojer EA, et al.
803   Polyunsaturated lipids regulate membrane domain stability by tuning membrane order.
804   Biophys J. 2016;110:1800–1810.

805   84.   Stillwell W, Shaikh SR, Zerouga M, Siddiqui R, Wassal SR. Docosahexaenoic acid
806   affects cell signaling by altering lipid rafts. Reprod Nutr Dev. 2005;45:559–579.

807   85.   Charest PG, Bouvier M. Palmitoylation of the V2 Vasopressin Receptor Carboxyl Tail
808   Enhances β-Arrestin Recruitment Leading to Efficient Receptor Endocytosis and
809   ERK1/ 2 Activation. J Biol Chem. 2003;278:41541–41551.

810   86.   Hawtin SR, Tobin AB, Patel S, Wheatley M. Palmitoylation of the Vasopressin V1a
811   Receptor Reveals Different Conformational Requirements for Signaling, Agonist-
812   induced Receptor Phosphorylation, and Sequestration. J Biol Chem. 2001;276:38139–
813   38146.

814   87.   Karnik SS, Ridge KD, Bhattacharya S, Khorana HG. Palmitoylation of bovine opsin
815   and its cysteine mutants in COS cells. Proc Natl Acad Sci U S A. 1993;90:40–44.

816   88.   Moffett S, Mouillac B, Bonin H, Bouvier M. Altered phosphorylation and desensitization
817   patterns of a human β2-adrenergic receptor lacking the palmitoylated Cys341. EMBO
818   J. 1993;12:349–356.

819   89.   Palmer TM, Stiles GL. Identification of threonine residues controlling the agonist-
820   dependent phosphorylation and desensitization of the rat A3 adenosine receptor. Mol
821   Pharmacol. 2000;57:539–545.

822 90. Pickering DS, Taverna FA, Salter MW, Hampson DR. Palmitoylation of the GluR6
823   kainate receptor. Proc Natl Acad Sci U S A. 1995;92:12090–12094.

824 91. Lally CCM, Bauer B, Selent J, Sommer ME. C-edge loops of arrestin function as a
825   membrane anchor. Nat Commun. 2017;8:1–12.

826 92. Cho D, Zheng M, Min C, Ma L, Kurose H, Park JH, et al. Agonist-induced endocytosis
827   and receptor phosphorylation mediate resensitization of dopamine D2 receptors. Mol
828   Endocrinol. 2010;24:574–586.

829 93. Lan H, Teeter MM, Gurevich V V, Neve KA. An intracellular loop 2 amino acid residue
830   determines differential binding of arrestin to the dopamine D 2 and D 3 receptors. Mol
831   Pharmacol. 2009;75:19–26.

832 94. Zhang X, Choi BG, Kim KM. Roles of dopamine D2 receptor subregions in interactions
833   with β-arrestin2. Biomol Ther. 2016;24:517–522.

834 95. Donthamsetti P, Gallo EF, Buck DC, Stahl EL, Zhu Y, Lane JR, et al. Arrestin
835   recruitment to dopamine D2 receptor mediates locomotion but not incentive
836   motivation. Mol Psychiatry. 2020;25:2086–2100.

837 96. Gallo EF, Meszaros J, Sherman JD, Chohan MO, Teboul E, Choi CS, et al.
838   Accumbens dopamine D2 receptors increase motivation by decreasing inhibitory
839   transmission to the ventral pallidum. Nat Commun. 2018;9:1–13.

840 97. Berger GE, Proffitt T-M, McConchie M, Yuen H, Wood SJ, Amminger GP, et al. Ethyl-
841   Eicosapentaenoic Acid in First-Episode Psychosis: A Randomized, Placebo-Controlled
842   Trial. J Clin Psychiatry. 2007;68:1867–1875.

843 98. Robinson DG, Gallego JA, John M, Hanna LA, Zhang JP, Birnbaum ML, et al. A
844   potential role for adjunctive omega-3 polyunsaturated fatty acids for depression and
845   anxiety symptoms in recent onset psychosis: Results from a 16 week randomized
846   placebo-controlled trial for participants concurrently treated with risperidone. Schizophr
847   Res. 2019;204:295–303.

848 99. Amminger GP, Schäfer MR, Schlögelhofer M, Klier CM, McGorry PD. Longer-term
849   outcome in the prevention of psychotic disorders by the Vienna omega-3 study. Nat
850   Commun. 2015;6:1–7.

851

852 **Tables**

853

Ratio	0 - 250 ns	250 - 500 ns	500 – 750 ns	750 ns - 1 µs
SD(h)PC$_{sn-1}$	0.97	1.69	2.95	2.42

| SD(h)PC $_{sn\text{-}2\,(DHA)}$	2.01	3.05	4.61	4.08
SD(p)PC $_{sn\text{-}1}$	1.49	1.48	1.48	1.63
SD(p)PC $_{sn\text{-}2\,(DPA)}$	1.47	1.95	2.28	2.33

Table 1. Evolution of lipid-protein contacts during MD simulations. The table shows the average relative proportion of lipid-protein contacts at four stages of the simulation. Contact ratios represent the number of atomic contacts between each SD(h)PC or SD(p)PC chain (i.e. sn-1 or sn-2) and the D2R, with respect to the number of contacts between saturated phospholipids (i.e. DPPC, DSPC, and PSM) and the protein (see Methods for more details).

	Ratio	0 - 250 ns	250 - 500 ns	500 - 750 ns	750 ns - 1 µs
DA	SD(h)PC$_{sn\text{-}1}$	1.16	0.98	1.00	0.81
	SD(h)PC $_{sn\text{-}2\,(DHA)}$	1.78	1.63	1.62	1.73
ARI	SD(h)PC $_{sn\text{-}1}$	0.97	1.46	1-65	1.67
	SD(h)PC $_{sn\text{-}2\,(DHA)}$	1.75	2.87	3.12	3.07

Table 2. Evolution of lipid-protein contacts during ligand-bound D2R simulations. The table shows the average relative proportion of lipid-protein contacts at four stages of the simulation. Contact ratios represent the number of atomic contacts between each SD(h)PC chain (i.e. sn-1 or sn-2) and the dopamine (DA)- or aripiprazole (ARI)-bound D2R, with respect to all saturated lipids (i.e. DPPC, DSPC and PSM) (see Methods for exact membrane composition and details on the calculation of these ratios).

Figure Legends
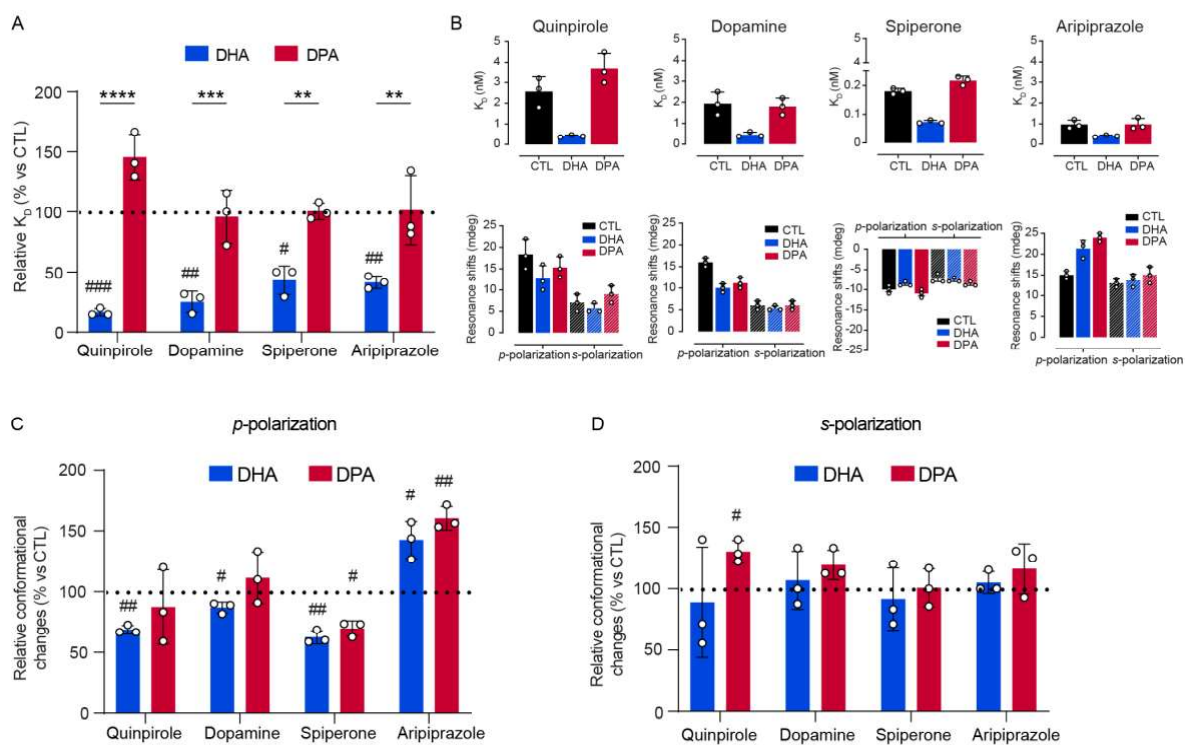
871 **Figure 1.** D2R binding affinity in PUFA-enriched cell membranes shown by PWR. (A) PUFA

872 effect on relative binding affinity of all ligands under DHA or DPA membrane enrichment. (B)

873 Dissociation constants (K_D) and maximum resonance shifts measured for each ligand. (C, D)

874 Relative receptor conformational changes, for *p*-polarization (C) and *s*-polarization (D). Data

875 are mean ± SD values from 3 independent experiments. Multiple comparisons were evaluated

876 by two-way ANOVA and Šídák's post hoc tests with **** $p<0.0001$, *** $p <0.001$, ** $p<0.01$, *

877 $p<0.05$. Comparisons to the control were evaluated by a one-sample t-test with ### $p <0.001$,

878 ## $p<0.01$, # $p<0.05$.
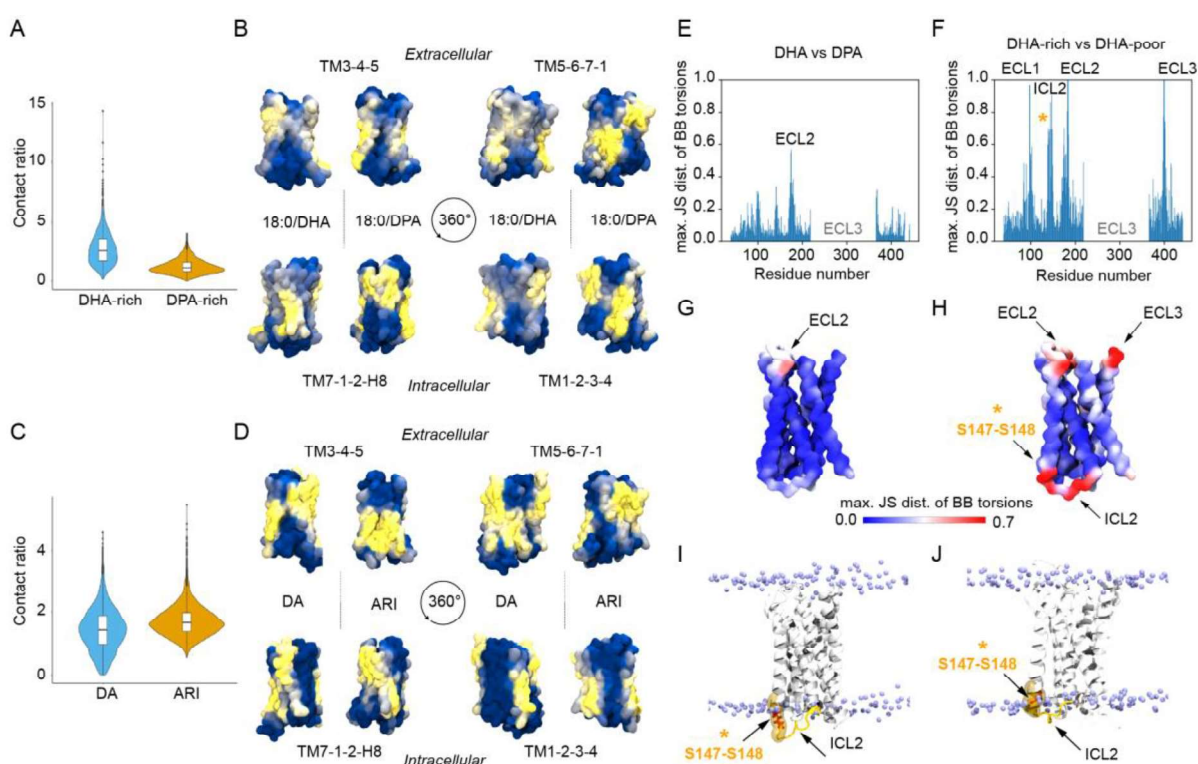
879

880 **Figure 2.** Lipid-protein contacts during MD simulations and effect on the structure of the D2

881 receptor. (A, C) Relative proportion of atomic lipid-protein contacts for the simulations of the

882 apo state of the D2R embedded in DHA- versus DPA-rich membranes (A), and the simulations

883 of dopamine- (DA) versus aripiprazole (ARI)-bound D2R embedded in DHA-rich membranes

884 (C). Specifically, figures depict the lipid-protein contact ratio of each SD(h)PC or SD(p)PC

885 chain versus all saturated lipids (i.e. DPPC, DSPC, and PSM) (see Methods for a detailed

886 description of these ratios). (B, D) Average lipid occupancy map for the simulations of the apo

state of the D2R embedded in DPA- versus DHA-containing phospholipids (B), and the simulations of dopamine- (DA) versus aripiprazole (ARI)-bound D2R embedded in DHA-rich membranes (D). The percentage of frames where SD(h)PC or SD(p)PC lipid molecules contacted the D2R is depicted in a blue (low) to yellow (high) color gradient mapped to the surface of the receptor. (E, F) Relative entropy analysis of the D2R depicted as the maximum value of the Jensen-Shannon (JS) distance of the protein backbone (BB) torsion angles (y-axis) for each residue (x-axis) across all MD simulation replicas. The JS distance is a way of measuring how different two probability distributions, in this case, ensembles of BB torsion angles, are across two systems. Thus, the higher the JS distance, the higher the difference between the two ensembles. The plot shows a relative entropy analysis for DHA- versus DPA-rich (E), and DHA-rich versus DHA-poor (F) systems. The peak highlighted by the orange asterisk corresponds to the region of helix 4 that follows intracellular loop 2 (ICL2), namely residues 146 to 150. Subpanels (G) and (H) display an averaged D2R structure with the former relative entropy values depicted in a blue to red color gradient mapped to the surface of the receptor. To facilitate the comparison between both sets of results, the maximum red color of the gradient encompasses all values ≥ 0.7. (I) and (J) show a representative snapshot of the DHA-poor and DHA-rich simulations, respectively. The D2R receptor and ICL2 are shown as white and orange cartoons, respectively. Serine residues S147 and S148 are shown as red sticks, within the 146 to 150 protein segment, which is highlighted by an orange transparent surface. Phospholipid phosphorous atoms are shown as purple beads to highlight the membrane boundaries.

909
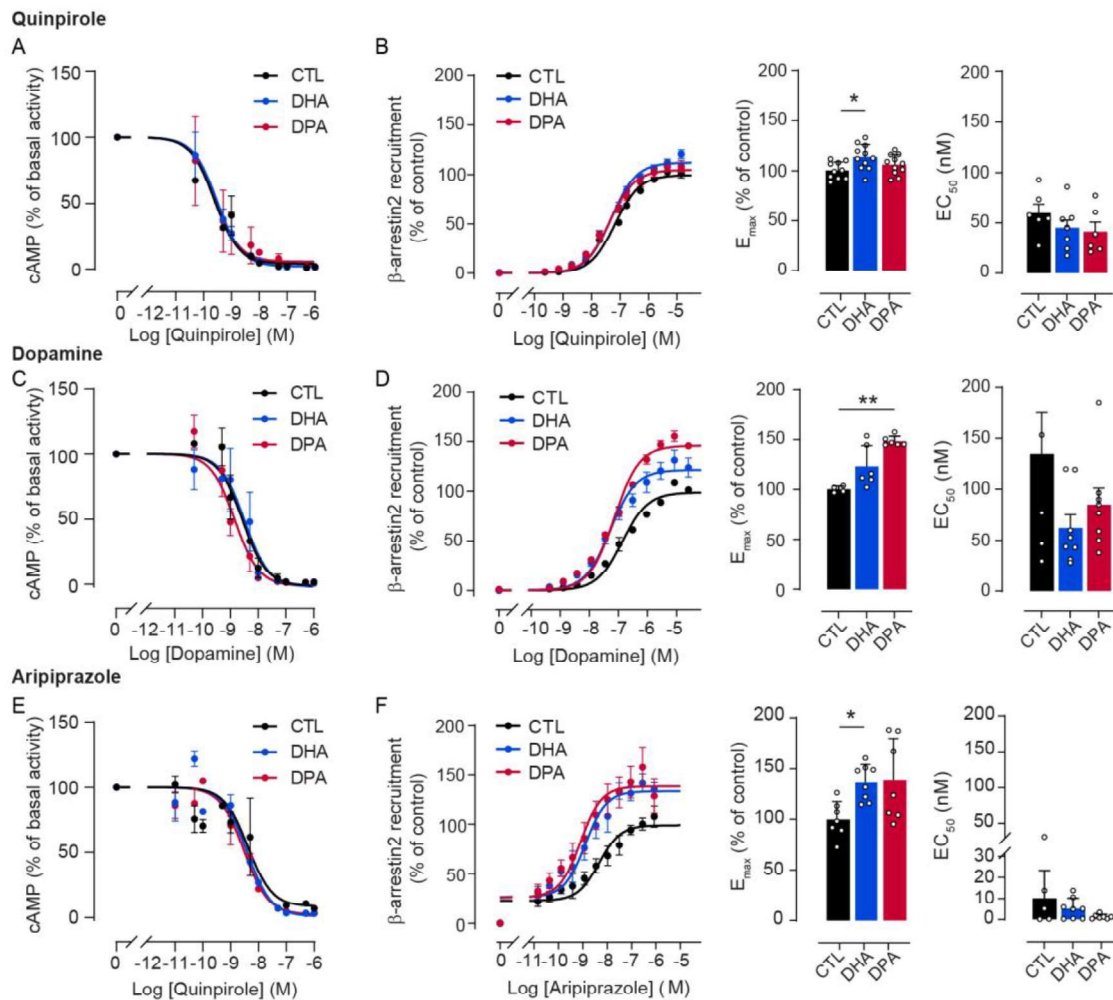
Figure 3. Forskolin-stimulated cAMP production and β-arrestin2 recruitment upon ligand stimulation and with different membrane PUFAs enrichment. (A, C, E) Dose-response experiments of cAMP production with the D2R ligands quinpirole (A), dopamine (C) and aripiprazole (E), on forskolin-stimulated cells incubated in the presence of 0.03% ethanol as control, 30 µM DHA and 30 µM DPA n-6. Values are expressed as the percentage of cAMP in the absence of agonist in n=3 independent experiments. (B, D, F) Quinpirole (B), Dopamine (D) and aripiprazole (F) activity on D2R-mediated β-arrestin2 recruitment in CHO-K1 cells expressing the DRD2L (left panel), and associated E_{max} (middle) and EC_{50} (right panel) under 30 µM PUFAs enrichment. Data are mean ± SD values from three independent experiments with **** $p<0.0001$, *** $p<0.001$, * $p<0.05$. cAMP assay and β-arrestin2 recruitment curves are mean ± SEM. Comparisons to the control were evaluated by a Kruskal-Wallis and Dunn's post-hoc tests.

922
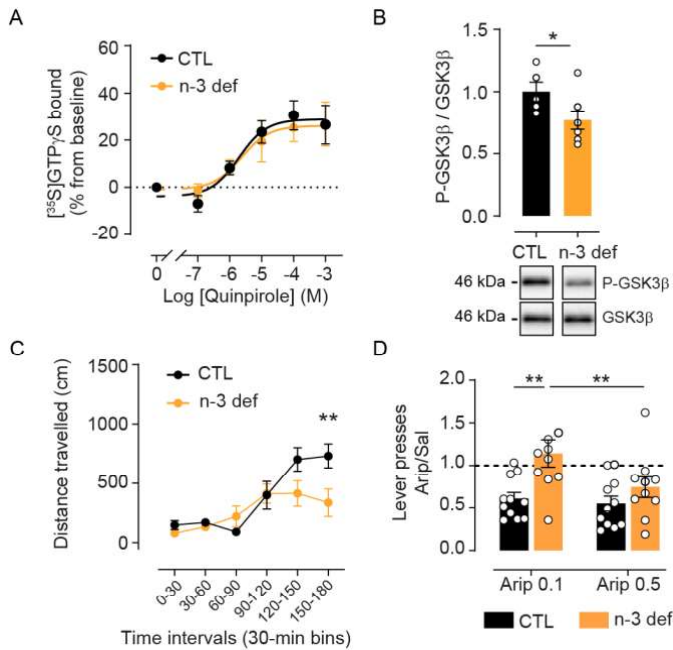
Figure 4. Effect of n-3 PUFA deficiency *in vivo* on D2R signalling and associated behaviors. (A) [^{35}S]GTPγS assay on nucleus accumbens extracts upon increasing concentrations of quinpirole from control (CTL) or n-3 PUFA deficient animals (n-3 def). CTL : logEC$_{50}$ = -5.22 ± 0.28 %, E$_{max}$ = 30.06 ± 3.47 % ; n-3 def : logEC$_{50}$ = -5.06 ± 0.29; E$_{max}$ = 28.15 ± 3.51 % (B) Western blots measuring the phosphorylation of GSK3β (P-GSK3β) relative to GSK3β levels. Bars represent the mean of 5 and 7 subjects for CTL and n-3 def respectively and error bars the SEM. *p<0.05 by Mann Whitney test. (C) Locomotor response to 1 mg/kg quinpirole administration is represented as the distance travelled in cm divided in 30 min intervals in control (CTL, n=10) or n-3 def (n=10) animals. ** p< 0.01 by two-way (RM) ANOVA test with a post-hoc Bonferroni test (D) Ratio of lever presses performed by animals under aripiprazole (0.1 or 0.5 mg/kg) over saline administration in a progressive ratio task in CTL (n=11) or n-3 def (n=10) animals. Data are mean ± SEM values. ** p< 0.01 by two-way (RM) ANOVA test with a post-hoc Bonferroni test.

Supplementary Methods :

Cell culture and treatment

Cells were maintained at 37°C under 5% CO2 in the following culture medium: DMEM (Dulbecco's modified Eagle's medium) Glutamax (InVitroGen) containing 10% of heat inactivated fetal bovine serum, 100 UI/ml penicillin and 0.1mg/ml streptomycin and supplemented with 100 µg/ml Hygromycin (InVitrogen), 15µg/ml Blasticidin (Cayla Invivogen) and 1 µg/ml Tetracycline (Sigma Aldrich). Upon reaching 80-90% confluence, in the same culture medium, cells were treated with 10 µM and 30 µM DHA or DPA or 0.03% and 0.01% ethanol (vehicle) respectively as control for 24h. After treatment, cells were dissociated by using an Enzyme-Free Cell Dissociation Solution (S-014-B, Merck Millipore) and washed twice in wash buffer (50 mM Tris-HCl, 50 mM NaCl, 2 mM EDTA, pH 7.5 at 20°C) by centrifugation at 500 $^\times$ g for 8 min at 20°C. Cell pellets were used either for Western blot analyses or for membrane preparation.

Membrane preparation

The cell pellets of HEK cells were resuspended in 10 ml of lysis buffer (10 mM Tris-HCl, 1 mM EDTA, pH 7.5 at 4°C) supplemented with anti-protease inhibitor cocktail (PIC; 1 µg/mL) (P8340, Sigma Aldrich) and incubated for 30 min in ice. The cell lysate was homogenized using a 10 ml glass-Teflon homogenizer with 30 gentle strokes. The resulting suspension was centrifuged at 183 $^\times$ g for 10 min at 4°C. The supernatant was collected and the residual pellet was washed twice by centrifugation successively in 5 and 2.5 ml of lysis buffer. The resulting supernatants were pooled and centrifuged at 48000 $^\times$ g for 30 min at 4°C. The pellet containing the membrane proteins was resuspended in binding buffer (50 mM Tris-HCl, 50 mM NaCl, 2 mM EDTA, 2 mM $CaCl_2$, pH 7.5 at 4°C) supplemented with PIC. Protein concentration was determined by using Bicinchoninic Acid (BCA) protein assay (Uptima, Montluçon, France) and membranes were diluted to 1 µg/µl in binding buffer.

Plasmon waveguide resonance (PWR)

Experiments were carried out at controlled room temperature, e.g. 23°C. The sensor consists in a 90° angle prism whose hypotenuse is coated with a silver layer (50 nm) and overcoated with silica (460 nm) and is in contact with the cell sample Teflon block, with an aperture of approximately 3 mm diameter through which the lipid bilayer is formed. This is placed on a rotating table mounted on a corresponding motion controller (Newport, Motion controller XPS; ≤ 1 mdeg resolution).

Formation of a planar lipid bilayer on the PWR sensor

The planar lipid bilayer is formed across the small aperture (~ 3 mm) in the Teflon PWR cell by fusing freshly sonicated small unilamellar vesicles (SUV, 3mg/ml) with the silica surface. SUVs were prepared by initially dissolving the appropriate amount of phospholipids in chloroform, to obtain the desired final concentration. A lipid film was then formed by removing the solvent using a stream of N_2 (g) followed by 3 h vacuum. The lipid film was dispersed in PBS and thoroughly vortexed to form multi-lamellar vesicles (MLVs). To form SUVs, the MLVs dispersion was sonicated 5 times during 10 minutes at 40Hz frequency just before use.

Immobilisation of cell fragments on the PWR sensor

The protocol for adhesion of cell fragments on silica (glass slides or PWR sensor) was adapted from reported work from Perez and collaborators [28]. The silica surface was washed with ethanol, cleaned and activated by Plasma cleaner for 2 min (Diener, Bielefeld, Germany). The silica surfaces were then incubated with a solution of poly-L-lysine (PLL, 0.1 mg/mL) for 40 minutes following wash with PBS buffer. Cells grown to less than 50% confluence were washed with PBS and covered with water to induce osmotic swelling of the cells. Immediately, the glass coverslip of the sensor was placed directly on top of cells. Pressure was applied for about 2 min on the glass slide or prism to induce cell rupture and caption of cell fragments. Then they were removed ripping off cell fragments containing specially the upper membrane. The glass slide or sensor was washed with PBS to remove cell debris and kept with buffer to prevent drying and loss of membrane protein activity. PWR measurements were performed right away. The PWR cell sample (volume capacity of 250 μL) was placed in contact with the prism and filled with PBS.

Partial purification and reconstitution of the dopamine D2 receptor in the lipid bilayer

D2R-expressing membranes from Pichia pastoris (gift from JL Banères) were used. All steps were performed at 4°C or on ice. Isolated membranes were diluted to 5 mg/ml with 50 mM Tris-HCl, pH 8, 500 mM NaCl, 5% glycerol, 1 mM PMSF, 0.1 mM TCEP, 10 mM imidazole. N-Dodecyl-β-D-maltoside (DDM) mixed with cholesteryl hemisuccinate (CHS) was added to a final concentration of 1%/0.2% DDM/CHS (w/v) and incubated for 15 min at 4°C. The suspension was centrifuged for 20 min at 120,000 x g. Solubilized receptor was purified by immobilized metal ion affinity chromatography (IMAC) on a Talon column (1 ml). The column was equilibrated in purification buffer (50 mM Tris-HCl, 500 mM NaCl, 5% glycerol, 1 mM PMSF, 0.1 mM TCEP, with 10 mM imidazole, 0.1%/0.02% DDM/CHS (w/v), pH 8). Solubilized proteins were loaded on the column (0.1 mL/min flow-rate) and washed in purification buffer until baseline was reached (UV absorbance 280 nm). After a washing step (50 mM Tris-HCl,

70   500 mM NaCl, 5% glycerol, 1 mM PMSF, 0.1 mM TCEP, 20 mM imidazole 0.1%/0.02%

71   DDM/CHS (w/v), pH 8), proteins were eluted by elution buffer (50 mM Tris-HCl, 500 mM NaCl,

72   5% glycerol, 1 mM PMSF, 0.1 mM TCEP, 250 mM imidazole, 0.1%/0.02% DDM/CHS (w/v),

73   pH 8) and eluted fractions containing protein were pooled. Enrichment of the D2R in the eluates

74   was verified by western blot (Fig. S4D) by assessing relative D2R (anti-D2R: Millipore Cat. No.

75   ABN462, 1/500) amounts as compared to total membrane extract with equal amounts of

76   protein loaded (2.5 μg).

77   After lipid bilayer formation, detergent-solubilized D2 receptor was reconstituted in the lipid

78   bilayer by the detergent-dilution method (see supplementary information for details). Briefly,

79   the receptor was purified in a DDM/CHS mixture at concentrations that are about 10 fold over

80   the critical micelle concentration (cmc) of DDM. Part of the detergent was then removed from

81   the sample by use of centricons (Merck Millipore) with a cutoff of 50 KDa. This consisted in

82   concentrating and reducing the initial volume of the solubilized protein by a factor of 5. The

83   insertion of a small volume (about 20 μL) of DDM/CHS solubilized protein into the PWR

84   chamber, leads to drastic and quick drop in the detergent concentration. If the detergent

85   concentration drops below the cmc during this step, this results in immediate positive PWR

86   shifts for both *p*- and *s*-polarisations with small changes in the Total Internal Reflection (TIR)

87   angle. In order to compare data among different experiments, data were normalized relative

88   to the amount of reconstituted protein in the membrane.

Ligand-induced receptor response

90   The method consisted in incrementally adding a specific dopamine D2 ligand to the cell and

91   monitor the PWR spectral changes. The first concentration point was chosen to be

92   approximately 1 order of magnitude lower than the published dissociation constant (K_D) value

93   for that ligand. Before each incremental concentration of ligand added, the system was left to

94   equilibrate. K_D values were obtained from plotting the resonance minimum position of the PWR

95   spectra (this reflects the receptor-ligand complex) as a function of ligand concentration in the

96   PWR cell and fitting to the hyperbolic function that describes the 1:1 binding of a ligand to a

97   receptor using GraphPad Prism (GraphPad Software). This was performed separately for data

98   obtained with the *p*- and *s*-polarization. The reported K_D is an average of the two values. The

99   spectral changes (equivalent to B_{max}) observed at saturating ligand concentrations for each

100 experimental condition were plotted. Multiple comparisons were evaluated by two-way ANOVA

101 and Šídák's post hoc tests. Comparisons to the control were evaluated by a one-sample t-test.

102

cAMP accumulation assays

104 D2R stably expressing HEK 293 (or CHO when indicated) cells were grown on PLL treated

105 12-well plates as described above. Upon reaching 80-90% confluence, cells were treated with

106 10 µM or 30 µM DHA or DPA n-6 or 0.03 % to 0.1 % ethanol (vehicle) as control for 24 h in the

107 culture medium. The medium was removed and cells were rinsed in DMEM before

108 pretreatment with 1 mM IsoButylMethylXanthine (IBMX, Sigma I5879) for 15min. Cells were

109 then stimulated for 30 min with the indicated concentrations of agonists Quinpirole (Tocris

110 1061), Dopamine (Sigma H8502) and Aripiprazole (Sigma SML0935) in the presence of 1 mM

111 IBMX and 10 µM Forskolin (Tocris 1099). Endogenous phosphodiesterase activity was

112 stopped by removing the medium and the addition of 0.1 M HCL (300 µl/well). After

113 centrifugation at 600 x g during 10 min, protein concentration of supernatants was quantified

114 by BCA. Cyclic AMP levels were determined in samples containing 10 µg of protein. The

115 production of cAMP was measured by using a cAMP Enzyme Immunoassay kit (Sigma,

116 CA200) as described by the manufacturer using Victor3 (Perkin Elmer) plate reader. The curve

117 fit was obtained by GraphPad Prism 5 (GraphPad Software, Inc.).

118

119 **Fluorescence anisotropy assay**

120 Fluorescence anisotropy (FA) was used to measure receptor-ligand binding reaction into

121 individual wells of black, 96-well Greiner Bio-One microplates in a final volume of 100µl. To

122 establish a saturation binding curve, the range of protein membrane concentration used was

123 from 1 to 25 µg in the presence of 10 nM of the antagonist NAPS-d2 ligand (L0002 red, Cisbio

124 Bioassays). The FA was measured on a Tecan Infinite M1000 Pro microplate reader

125 (Männedorf, Switzerland). Excitation was set at 590 ± 5 nm and emission was collected at 665

126 ± 5 nm bandpass filters for the Texas Red.

127 The non-specific binding was obtained from membranes that did not express the receptor and

128 the total binding was measured with D2R-expressing membranes. The binding curve was

129 performed on the total amount of proteins measured in the sample. The non-specific binding

130 curve was fitted with a Simple-linear regression in GraphPad Prism (GraphPad Software, San

131 Diego, CA) and the total binding curve was fitted with a One site – total binding curve in

132 GraphPad Prism. The specific binding was determined by subtracting the non-specific curve

133 to the total binding curve and the final specific binding curve was fitted with a One site – specific

134 binding model in GraphPad Prism. The latter was used to determine relative K_D values via

135 separated saturation binding curves in at least three independent experiments and are

136 reported as mean ± SEM. The lower the value, the higher the affinity.

137

138 **β-Arrestin2 recruitment assay**

139 β-arrestin2 recruitment was assessed using the PathHunter© express DRD2L CHO-K1 Beta

140 arrestin GPCR Assay (DiscoverX, Fremont, CA). In brief, cells were plated into 96-well white-

141 walled assay plates in a volume of 90 µl of Cell Plating Reagent (DiscoverX). They were

142 incubated 24 h at 37 °C, 5 % CO_2.The next day, PUFAs (Ethanol 0.01% as control vehicle,

143 DHA, and DPA n-6) were prepared at 10X concentration (300 µM) in Cell Plating Reagent and

144 10 µL was added to the cells for 24h at 37 °C, 5 % CO_2. Serial dilutions (11x) ranging from 154

145 to 0.0026 µM, 281 to 0.0046 µM and 9.35 to 0.000157 µM, of Quinpirole, Dopamine and

146 Aripiprazole respectively, were prepared and 10 µl of each concentration was added for 90

147 minutes. Luminescence was measured at 1 h post PathHunter© detection reagent addition

148 using Victor3 plate reader (Perkin Elmer 0.5-s/well integration time). Data were normalized to

149 control treated with the highest concentration of ligand (100%). This control value corresponds

150 to Top best fit value determined by non-linear fit of standard slope. Data were fitted to a three-

151 parameter logistic curve to generate EC_{50} and E_{max} values (Prism, version 5.0, GraphPad

152 Software, Inc., San Diego, CA). EC_{50} and % E_{max} values are the result of three independent

153 experiments performed in duplicate.

154

155 **Behavioral experiments**

156 All animal care and experimental procedures were in accordance with the INRAE Quality

157 Reference System and to French legislations (Directive 87/148, Ministère de l'Agriculture et

158 de la Pêche) and European (Directive 86/609/EEC). They followed ethical protocols approved

159 by the Region Aquitaine Veterinary Services (Direction Départementale de la Protection des

160 Animaux, approval ID: B33-063-920) and by the animal ethic committee of Bordeaux CEEA50.

161 Every effort was made to minimize suffering and reduce the number of animals used.

162 C57BL/6J mouse lines from Janvier Laboratories (Robert Janvier, Le Genest St-Isle France)

163 were used in this study. Mice were housed in groups of 5-10 animals in standard polypropylene

164 cages and maintained in a temperature and humidity-controlled facility under a 12:12 light-dark

165 cycle (8:00 on) with *ad libitum* access to water and food.

166 **Operant conditioning:**

167 Animals were food-restricted in order to maintain them at 85-90% of their ad libitum weight and

168 exposed to one session (1 hour) each day, 5-7 days per week. A pavlovian training followed

169 by fixed and random ratio training were performed in order to make the animals reach an

170 acquisition criterion (i.e. the number of lever presses and rewards earned) before performing

171 the motivational task per se as previously described [14]. In the motivational task, namely the

172 progressive ratio times 2 (PRx2) schedule, the number of lever presses required to earn a

173 reward was doubled respective to the previous one obtained. Mice were tested multiple times
174 in PRx2 with RR20 sessions intercalated between each PR tasks.

Spontaneous locomotion:

176 Animals were transferred individually to small Plexiglas cages (10 cm wide, 20 cm deep, 12
177 cm tall) equipped with a video tracking system (Smart, Panlab, Barcelona, Spain) allowing the
178 recording of total distance travelled (cm) as a measure of spontaneous locomotor activity in
179 basal condition for one hour.

Western blot

181 The following primary antibodies were used: 1:700 rabbit anti-βArr2 (Cell signaling Cat. No.
182 3857); 1:1000 rabbit anti-GSK3β (Cell signaling Cat. No. 12456); 1:1000 rabbit anti-P-GSK3β
183 (Cell signaling Cat. No. 5558); 1:10000 mouse anti-tubulin (Merck Cat. No. T5168).

184

Cell Membrane preparation for Microarray and [^{35}S]GTPγS autoradiography

186 Tissue samples were homogenized using a Teflon-glass grinder (Heidolph RZR 2020) and a
187 disperser (Ultra-Turrax® T10 basic, IKA) in 20 volumes of homogenized buffer (1 mM EGTA,
188 3 mM MgCl2, and 50 mM Tris-HCl, pH 7.4) supplemented with 250 mM sucrose. The crude
189 homogenate was subjected to a 3,000 rpm centrifugation (AllegraTM X 22R centrifuge,
190 Beckman Coulter) for 5 min at 4°C, and the resultant supernatant was centrifuged at 14,000
191 rpm (Microfuge® 22R centrifuge, Beckman Coulter) for 15 min (4 °C). The pellet was washed
192 in 20 volumes of homogenized buffer and re-centrifuged under the same conditions. The
193 homogenate aliquots were stored at -80 °C until they were used. Protein concentration was
194 measured by the Bradford method and adjusted to the required concentrations.

Lipid analyses

196 Gas chromatography on a HewlettPackard Model 5890 gas chromatograph (Palo Alto, CA,
197 USA) was employed to analyze fatty acid methylesters (FAMEs) using aCPSIL-88 column (100
198 m×0.25 mm internal diameter; film thickness 0.20 µm; Varian, Les Ulis, France). Hydrogen
199 was used as a carrier gas (inlet pressure, 210 kPa). The oven temperature was maintained at
200 60 °C for 5 min, then increased to 165 °C at 15 °C/min and held for 1 min, and then to 225 °C
201 at 2 °C/min and finally held at 225 °C for 17 min. The injector and the detector were maintained
202 at 250 °C and 280 °C, respectively. FAMEs were identified by comparison with commercial
203 and synthetic standards and the data were computed using the Galaxie software (Varian). The

204   proportion of each fatty acid was expressed as a percentage of total fatty acids to allow the

205   comparison of lipid composition in different cell culture conditions.

206 **Statistical analyses**

207   Statistical analyses were conducted using Prism 6 software (GraphPad Software, La Jolla, CA,

208   USA). Two-tailed unpaired Student's t-test or Mann Whitney test were used to assess

209   differences between two groups. Multiple comparisons in Fig.1 were evaluated by two-way

210   ANOVA and Šídák's post hoc tests and comparisons to the control were evaluated by a one-

211   sample t-test. Two-way RM ANOVA followed by post-hoc Bonferroni tests were used for

212   repeated measures. Differences were considered significant for $p < 0.05$.

213

214

215

216

217

218

219

220

221

222

223

224

225

226

227

228

229

230

231

232 **Supplementary Figures :**

233

234 Figures S1 - S8

235
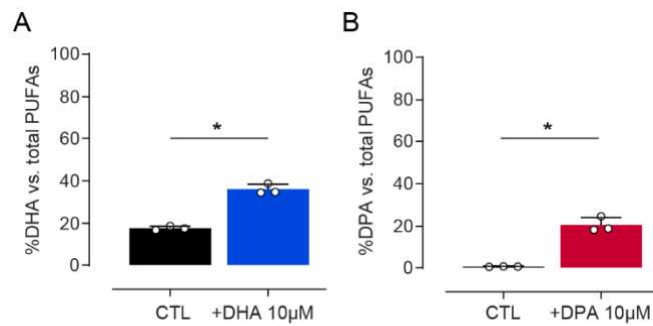
236

237

238 **Supplementary Figure S1. PUFAs enrichment in HEK cells.** HEK cells were incubated with DHA (A)
239 or DPA (B) at 10 µM concentration. Each PUFA enrichment is compared to control cells incubated with
240 vehicle only (0.03 % ethanol). Bars represent the mean average of three independent experiments and
241 error bars represent the standard deviation (SD). * $p < 0.05$ by one-tailed Mann-Whitney test.

242
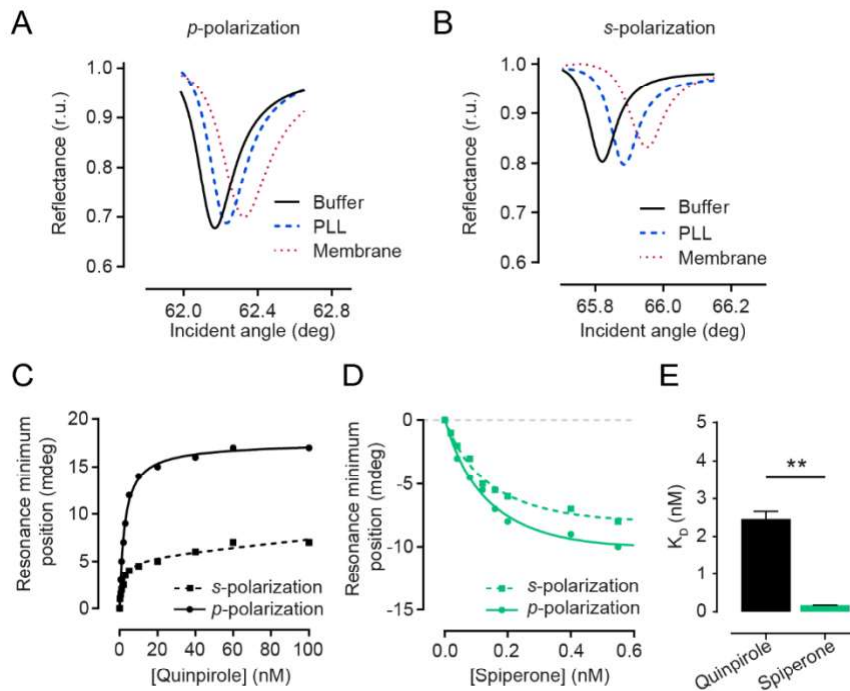
Supplementary Figure S2. Ligand binding on cell membrane fragments on the PWR sensor.
Capture of cell membrane fragments containing the D2R following PLL treatment of the PWR sensor
followed by PWR using *p*- and *s*-polarization. (**A and B**) Representative PWR spectra following sensor
coating with polylysine (PLL; blue) and cell membrane fragment capture (red) obtained with *p*- (A) and
s- (B) polarized light, respectively. (**C and D**) Quinpirole (**C**) and spiperone (**D**) were incrementally added
to the proteolipid membrane and the shifts in the resonance minimum position followed. The data were
fitted with a hyperbolic binding equation that describes total binding to a single site in the receptor (more
details in Materials and Methods). (**E**) Affinity binding of quinpirole and spiperone calculated from (**C**)
and (**D**) respectively. ** $p < 0.01$ by two-tailed unpaired t-test.

252

253
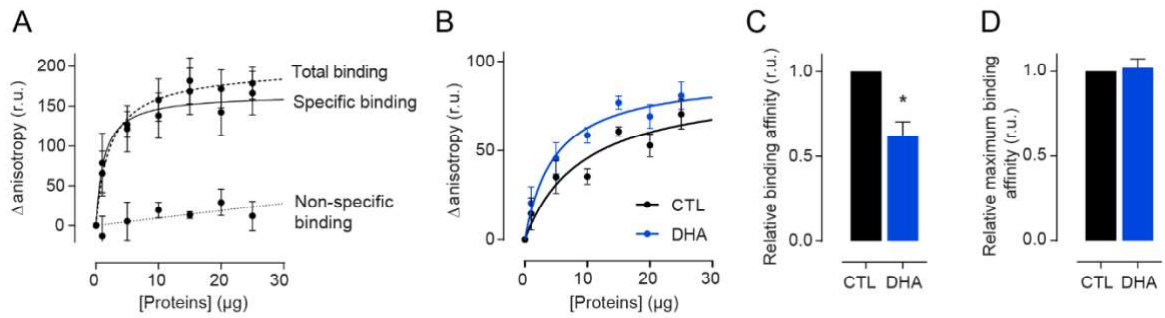
254
255 **Supplementary Figure S3. Impact of membrane DHA on D2R ligand binding measured by**
256 **fluorescence anisotropy. (A)** Fluorescence anisotropy measurement of NAPS-d2 binding on D2R-
257 expressing membranes (total binding) or non-expressing membranes (non-specific binding). **(B)**
258 Antagonist (NAPS-d2) binding to control and DHA-enriched membranes. **(C)** Fold change of ligand
259 affinity to D2R in DHA-enriched membranes compared to control membranes. **(D)** Maximum relative
260 binding affinity to D2R in DHA-enriched membranes. Data are mean ± SEM from three independent
261 experiments with * p<0.05 by two-tailed unpaired t-test.
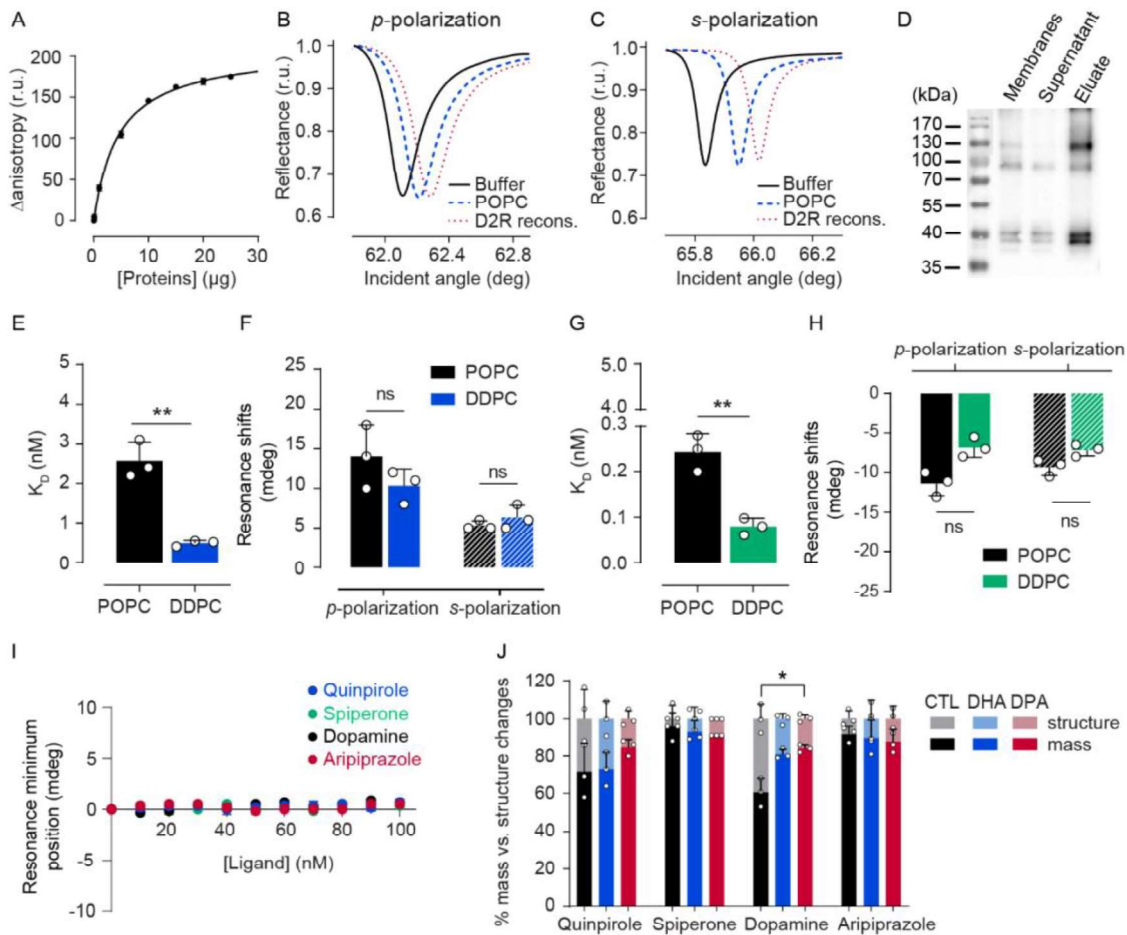
262

263

264 **Supplementary Figure S4. Impact of DHA on ligand binding to D2R partially purified and**
265 **reconstituted in model membranes shown by PWR. (A)** Fluorescence anisotropy measurement of
266 NAPS-d2 binding to partially purified D2R (total binding). **(B and C)** Representative PWR spectra
267 following supported POPC lipid membrane formation (blue) and D2R membrane reconstitution (red) for
268 *p*- (B) and *s*-polarized (C) light, respectively. **(D)** The D2R was partially purified from membrane extracts
269 and the enrichment of the D2R in the eluates was verified by western blot with an antibody anti-D2R. **(E**
270 **and F)** Effect of DHA on quinpirole affinity to D2R **(E)** and quinpirole-induced receptor conformational
271 changes **(F)** in reconstituted lipid model systems composed of POPC and double chain DHA-PL. **(G and**
272 **H)** Effect of DHA on spiperone affinity to D2R **(G)** and spiperone-induced receptor conformational
273 changes **(H)** in reconstituted lipid model systems. (I) Quinpirole, spiperone, dopamine and aripiprazole
274 were incrementally added to cell membrane fragments without D2R. (J) Mass and structural changes
275 contributions of the PWR spectral shifts observed upon ligand binding to the D2R in cell membrane
276 fragments enriched or not with PUFAs (at saturating ligand concentrations) determined by a graphical
277 analysis. Data are mean ± SD values from at least three independent experiments with ** $p<0.01$ by
278 two-tailed unpaired t-test (E and G) and * < 0.05 by Kruskal-Wallis and Dunn's post hoc test (J).
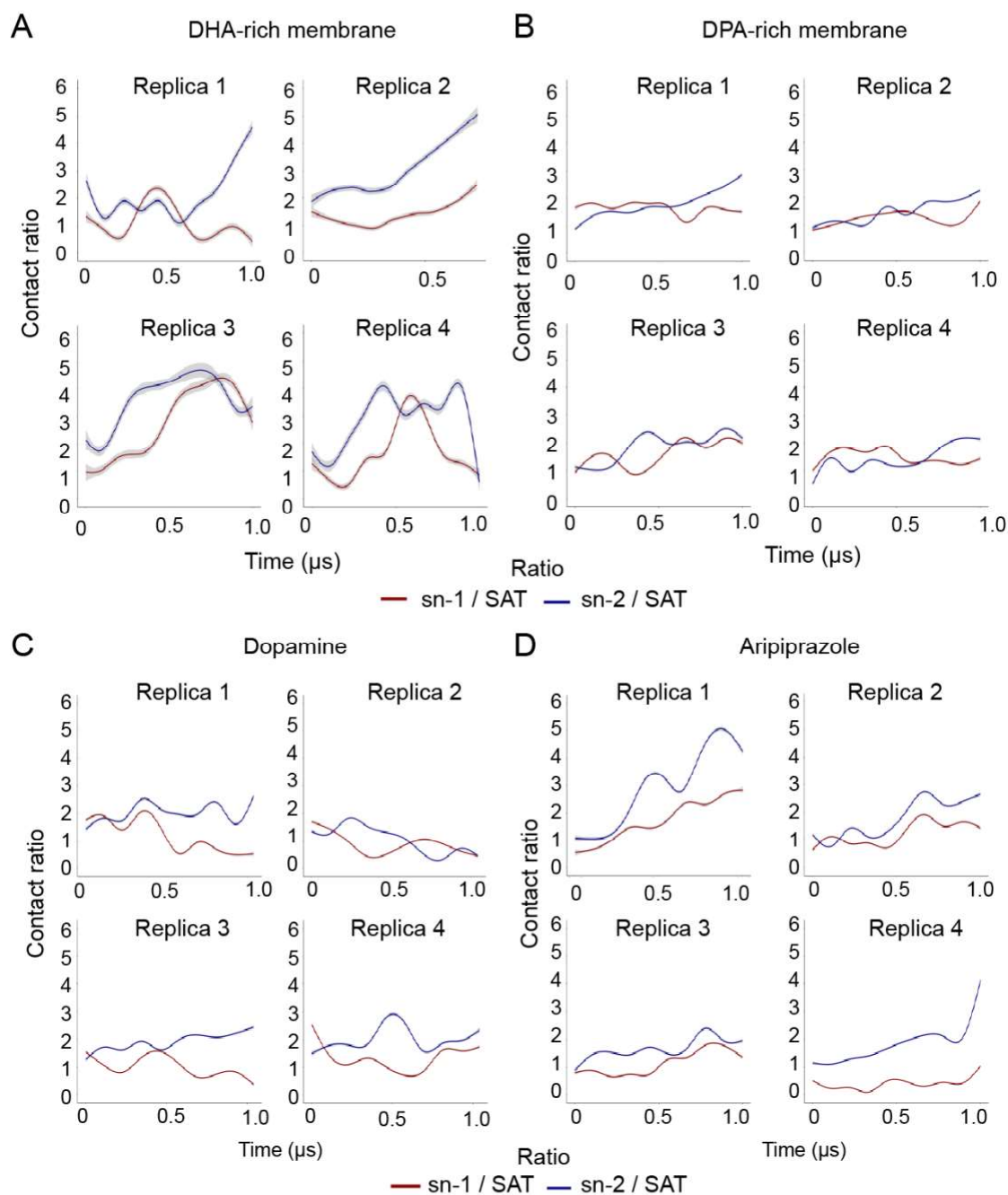
Supplementary Figure S5. Lipid-protein contacts during MD simulations. Relative proportion of atomic lipid-protein contacts (y-axis) over time (x-axis) for the simulations of the apo state of the D2R embedded in DHA- (A) versus DPA-rich (B) membranes, and the simulations of dopamine- (C) versus aripiprazole-bound D2R (E) embedded in DHA-rich membranes. Specifically, figures depict the contact ratio of each SD(h)PC or SD(p)PC chain versus all saturated lipids (i.e. DPPC, DSPC, and PSM) in the system (i.e. sn-1 / SAT and sn-2 / SAT) is depicted (see Methods for a detail description of these ratios).

287
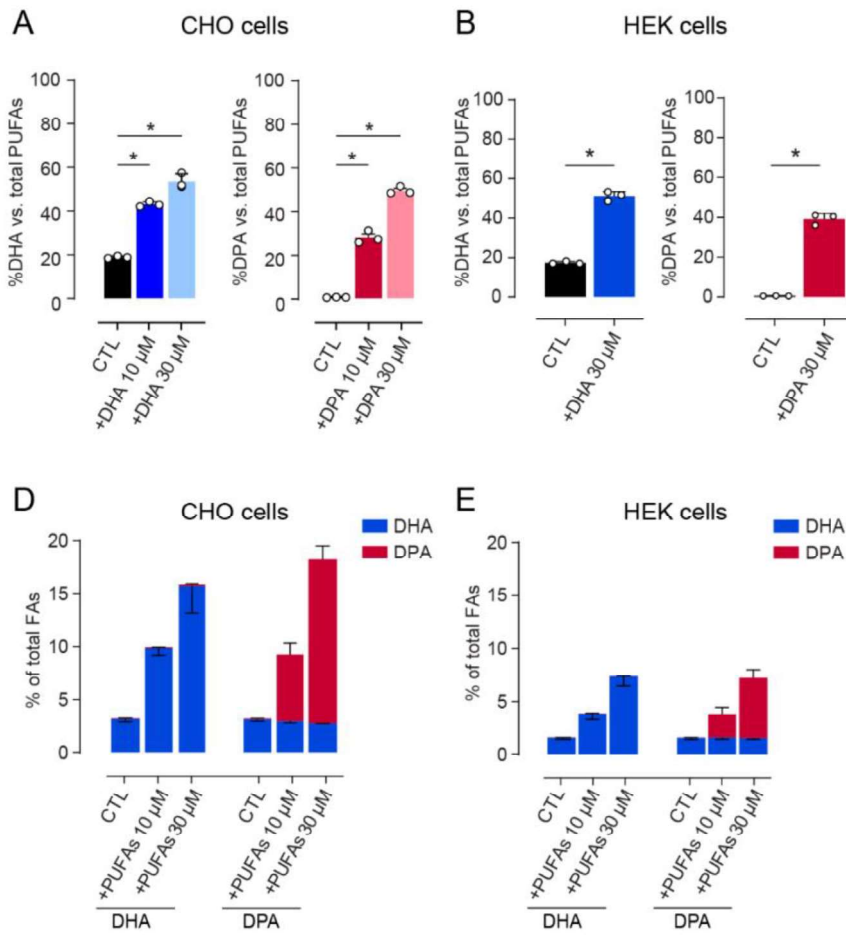
**Supplementary Figure S6. PUFAs enrichment in CHO and HEK cells. (A)** DHA and DPA incorporation in CHO cells through incubations at 10µM or 30µM. **(B)** DHA and DPA incorporation in HEK cells through incubations at 30µM. (C) Cumulative PUFA incorporation in CHO cells through incubations at 10µM or 30µM. (D) Cumulative PUFA incorporation in HEK cells through incubations at 10µM or 30µM. Bars represent the mean average of three independent experiments and error bars represent the standard error of the mean (SEM). * $p < 0.05$ by one-tailed Mann-Whitney test.

cAMP production

A Quinpirole (PUFAs 10µM; HEK cells) **B** **C** Quinpirole (PUFAs 30µM; CHO cells)

β-arrestin2 recruitment

D Quinpirole (PUFAs 10µM; CHO cells)

E Dopamine (PUFAs 10µM; CHO cells)

F Aripiprazole (PUFAs 10µM; CHO cells)

294
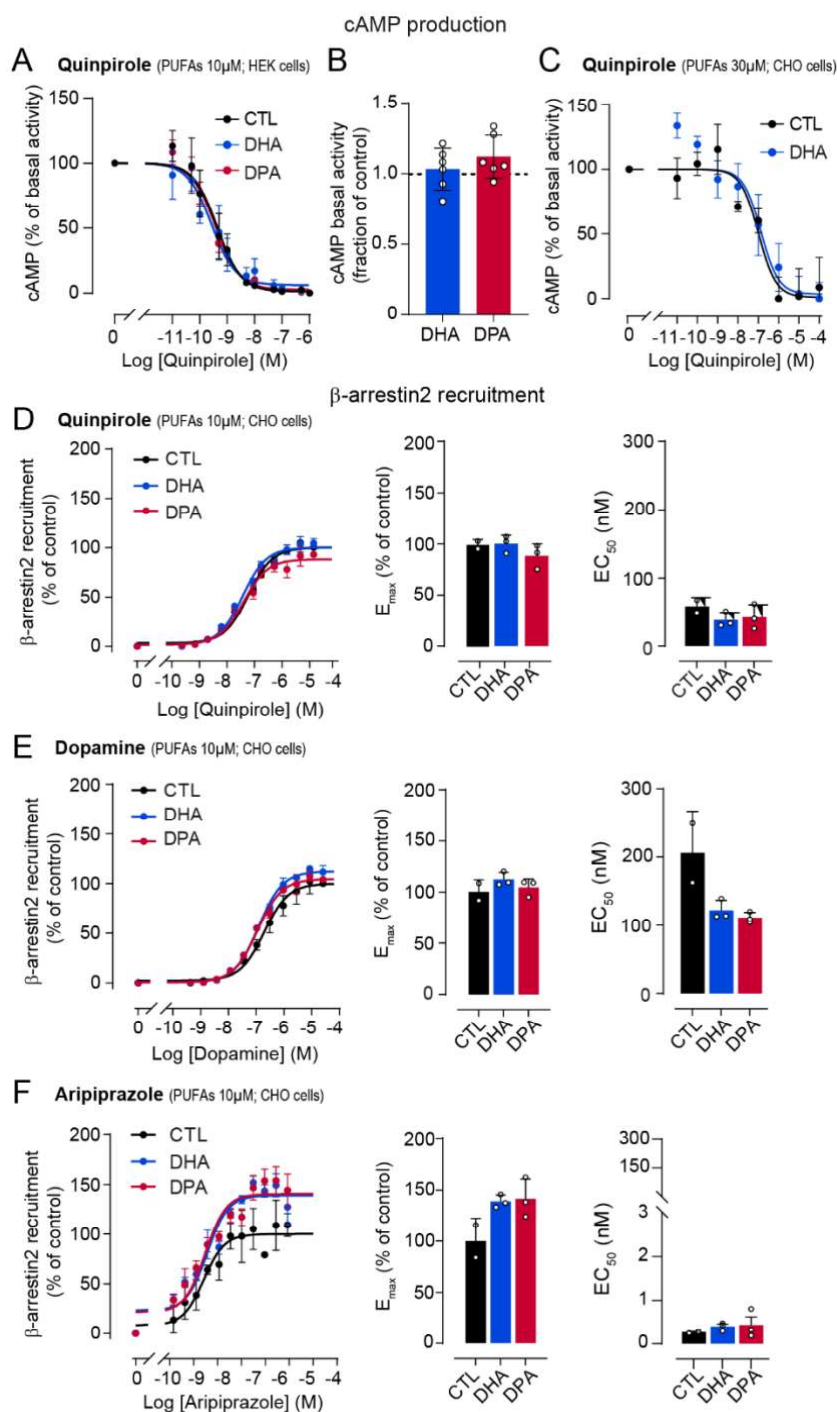
Supplementary Figure S7. cAMP inhibition and β-arrestin2 recruitment by the D2R upon stimulation by different ligands in cells. (A) Dose-response experiments of cAMP production with the D2R ligand quinpirole on forskolin-stimulated HEK cells incubated in the presence of 0.03% ethanol as control, 10 µM DHA or 10 µM DPA. **(B)** Effect of 30 µM PUFA enrichment on basal forskolin-induced cAMP production. **(C)** Dose-response experiments of cAMP production with the D2R ligand quinpirole on forskolin-stimulated CHO cells incubated in the presence of 0.03% ethanol as control or 30 µM DHA **(D)** Quinpirole activity on β-arrestin2 recruitment at the D2R in CHO-K1 cells expressing the DRD2L (left), and associated E_{max} (middle) and EC_{50} (right) under 10 µM incubation of either PUFA. **(E)** Dopamine activity on β-arrestin2 recruitment at the D2R in CHO-K1 cells expressing the DRD2L (left), and associated E_{max} (middle) and EC_{50} (right) under 10 µM incubation of either PUFA. **(F)** Aripiprazole activity on D2R mediated β-arrestin2 assay in CHO-K1 cells expressing the DRD2L (left), and associated E_{max} (middle) and EC_{50} (right) under 10 µM incubation of either PUFA. * $p < 0.05$, ** $p < 0.01$ by two-tailed unpaired t-test. Data are mean ± SD values from three independent experiments with ****

308   p<0.0001, *** p <0.001, * p<0.05. cAMP assay and β-arrestin2 recruitment curves are mean ± SEM.

309   Comparisons to the control were evaluated by a Kruskal-Wallis and Dunn's post-hoc tests.
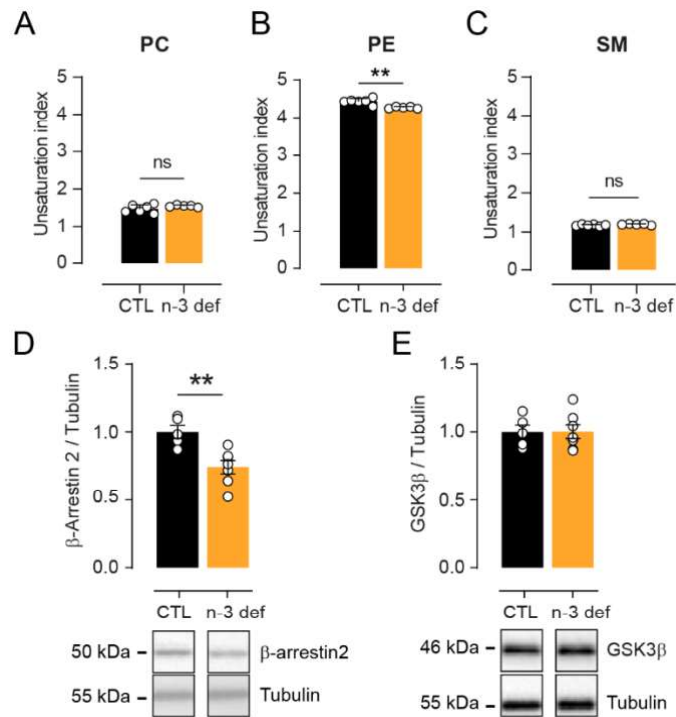
310

311

312 **Supplementary Figure S8. Expression of ꞵarrestin-2 and GSK3ꞵ in n-3 deficient mice (n-3 def).**
313 **(A, B, C)** Unsaturation index in mice corresponding to the average number of double bonds per fatty
314 acid present in total PUFAs ([percentage of each lipid]x[number of double bounds/number of fatty acid
315 species per lipid].**(D)** and **(E)** Expression of ꞵarrestin2 (A) and GSK3ꞵ (B) by western blot normalized
316 to the intensity of tubulin expression. Bars represent the mean of five and seven subjects for CTL and
317 n-3 def respectively and error bars the SEM. **p<0.01 by Mann Whitney test.
318

	CTL	DHA 10μM	DPA 10μM	CTL	DHA 30μM	DPA 30μM
Quinpirole	9.50 ± 0.12	9.39 ± 0.25	9.48 ± 0.20	9.40 ± 0.18	9.51 ± 0.08	9.62 ± 0.20
Dopamine	-	-	-	8.70 ± 0.12	8.54 ± 0.20	8.85 ± 0.21
Aripiprazole	-	-	-	8.08 ± 0.25	8.36 ± 0.16	8.46 ± 0.10

319

320 **Supplementary Table S1**. pIC$_{50}$ values (as mean ± SEM) from dose-response experiments of cAMP
321 production on forskolin-stimulated cells incubated in the presence of 0.03% ethanol as control (CTL),
322 10 μM DHA and 10 μM DPA or 30 μM DHA and 30 μM DPA upon quinpirole, dopamine and aripiprazole
323 stimulation of the D2R.

324

325

	Percentage (%)					
Model membrane	CHL1	DPPC (diC16:0)	DSPC (diC18:0)	DOPC (diC18:1)	SD(h)PC (C18:0 / C22:6)	SD(p)PC (C18:0 / C22:5)	PSM (C18:1 / C16:0)
DHA-rich	33	14	5	11	13	0	24
DPA-rich	33	14	5	11	0	13	24

326

327 **Supplementary Table S2. Lipid composition of the model membranes used in MD simulations.**
328 CHL1: cholesterol, DPPC: 1,2-dipalmitoyl-sn-glycero-3-phosphocholine, DSPC: 1,2-distearoyl-sn-
329 glycero-3-phosphocholine, DOPC: 1,2-dioleyl-sn-glycero-3-phosphocholine, SD(h)PC: 1-stearoyl-2-
330 docosahexaenoyl-sn-glycero-3-phosphocholine, SD(p)PC: 1-stearoyl-2- docosa(p)entaenoyl -sn-
331 glycero-3-phosphocholine, PSM: sphingomyelin.